Glacial isostatic adjustment and post-seismic deformation in Antarctica

Wouter van der Wal[1,2]*, Valentina Barletta[3], Grace Nield[4,5] and Caroline van Calcar[1,6]

[1]Faculty of Aerospace Engineering, Delft University of Technology, Kluyverweg 1, 2629 HS Delft, The Netherlands

[2]Department of Geosciences and Remote Sensing, Delft University of Technology, Stevinweg 1, 2628 CN Delft, The Netherlands

[3]DTU Space, National Space Institute, Geodynamics Department, Technical University of Denmark, Elektrovej, 328, 016, 2800 Kongens Lyngby, Denmark

[4]Department of Geography, Durham University, Lower Mountjoy, South Road, Durham DH1 3LE, UK

[5]School of Geography, Planning, and Spatial Sciences, University of Tasmania, Hobart, Tasmania 7001, Australia

[6]Institute for Marine and Atmospheric Research Utrecht, Utrecht University, Utrecht, 3508 TA, The Netherlands

WvdW, 0000-0001-8030-9080

*Correspondence: w.vanderwal@tudelft.nl

Abstract: This chapter reviews glacial isostatic adjustment (GIA) and post-seismic deformation in Antarctica. It discusses numerical models and their inputs, and observations and inferences that have been made from them. Both processes are controlled by mantle viscosity but their forcings are different. Ongoing GIA induced by the loss of ice since the last glacial maximum (LGM) could have amounted to 5–15 m of global sea-level rise. However, mantle viscosity is so low in parts of West Antarctica (*c.* 10^{18} Pa s) that changes in ice thickness over the last centuries and decades have controlled the current uplift rates there. The uplift due to GIA has promoted ice-sheet stability since the LGM, and in West Antarctica GIA is a significant negative feedback on the current decline of the ice sheet. Post-seismic deformation following the 1998 earthquake near the Balleny Islands south of New Zealand has been detected in global navigation satellite system (GNSS) data and compared to model outputs. The best-fitting viscosity for this area is *c.* 10^{19} Pa s, similar to GIA-based estimates for the Antarctic Peninsula. Future work should focus on unifying descriptions of viscosity across geodynamic models, and integrating information from seismic, gravity, experimental and geological data.

The mantle in Antarctica plays an important role in changing the elevation of the bedrock through forces applied to the base of the lithosphere, including convective flow of the mantle (dynamic topography), tectonics, heating and cooling of the lithosphere, and load redistribution at the surface (Paxman *et al.* 2019; Paxman 2021, this volume). Loading of the surface can be caused by changes in ice-sheet and snow thickness, sedimentation and erosion, sea-level changes, and changes in pressure due to oceanic and atmospheric currents and tides. Here we focus on the secular changes induced by the changing surface loading of the ice sheet and the stress redistribution caused by earthquakes. The adjustment of the Earth following growing or melting ice sheets is termed glacial isostatic adjustment (GIA) and is mostly measurable on a timescale from decades to millennia.

The adjustment of the Earth's crust and mantle after slip on the fault plane of an earthquake is called post-seismic relaxation; it is mostly measurable on a time frame from years to decades. Both are governed by the resistance to flow of the mantle, and numerical models rely on a similar description of the rheology of the mantle. Both processes can lead to vertical and horizontal motion that is linear or quasi-linear in global navigation satellite system (GNSS) time series (Scheinert *et al.* 2021, this volume). Post-seismic deformation is only detectable following large earthquakes, and only a few of these have occurred recently enough for them to have been measured in GNSS time series. In agreement with Scheinert *et al.* (2021, this volume), we will use the general term GNSS, which encompasses all global systems, even though most GNSS data on Antarctica are obtained from GPS receivers.

The response of the solid Earth to loading change can be instantaneous with respect to the forcing, in which case it is governed by the elastic properties of the crust and mantle that can be characterized, for example, by Young's modulus. The elastic deformation due to present-day surface-load changes is commonly applied as a correction to GNSS measurements (Scheinert *et al.* 2021, this volume). The solid Earth also shows a delayed response to the forcing, driven by the viscoelastic properties of the mantle. In this chapter, we focus on this viscoelastic behaviour. Modelling of the response of the solid Earth generally includes the elastic effect that occurs instantaneously at the moment of loading, as well as the delayed viscous effect (e.g. Peltier 1974).

Antarctica is particularly interesting for GIA studies as there are substantial variations in the Earth's structure beneath East and West Antarctica, as shown by the lower than average seismic velocities beneath West Antarctica. To first order, low seismic velocities correspond to high temperatures (e.g. Goes and van der Lee 2002). Therefore, West Antarctica is inferred to have a warmer and, hence, weaker mantle, while the East Antarctic Craton is underlain by a colder and stiffer mantle (Berg *et al.* 1989; Morelli and Danesi 2004; Hansen *et al.* 2014; Martin *et al.* 2014; An *et al.* 2015; Burton-Johnson *et al.* 2020; Wiens *et al.* 2021, this volume). Thus, it is expected that GIA and post-seismic deformation would proceed at a different rate in West Antarctica than in East Antarctica, and simulations should take this into account.

The following section of this chapter is dedicated to GIA. A brief introduction to the topic is given and the physics associated with the processes are discussed, together with the main results derived from existing GIA models. Readers familiar with GIA processes and models may wish to skip this part. For more details, the review paper by Whitehouse (2018) may be consulted. The section continues with a review of results of GIA models in Antarctica, focusing on deglaciation since the last glacial maximum (LGM) and inferences of mantle viscosity. Particular attention is paid to the interaction between GIA and ice-sheet dynamics. Post-seismic deformation is discussed in the third section of this chapter: specifically, the occurrence of earthquakes, a description of mantle flow and the results of post-seismic deformation following the 1998 earthquake. Finally, conclusions are presented and potential future work for GIA and post-seismic deformation are outlined.

From: Martin, A. P. and van der Wal, W. (eds) *The Geochemistry and Geophysics of the Antarctic Mantle*.
Geological Society, London, Memoirs, **56**,
https://doi.org/10.1144/M56-2022-13

GIA

The growing concern about climate change is generating great interest in the rate at which ice-covered regions are losing mass and transferring water to the oceans. Estimates of current ice-mass changes are produced by analyses that incorporate geodetic and glaciological observations (Shepherd *et al.* 2018). However, to predict future ice-sheet melt we also need physical models of ice dynamics. In this context, the behaviour of the solid Earth is particularly important. Ice change triggers GIA, which in turns affects the ice dynamics. For example, a rising coastal region can lead to a displacement of the grounding line, affecting the way in which the oceans interact with land-based ice (Thomas 1979; Oerlemans 1980).

The GIA process is not only relevant for ice sheet–solid Earth feedback, as the GIA signal is present in geodetic observations of present-day uplift and gravity change rate. For example, in GRACE (Gravity Recovery and Climate Experiment) satellite measurements of mass change in Antarctica, GIA makes up about one-third of the total signal (Shepherd *et al.* 2018). Therefore, in order to recover the signal due to the present-day ice melt, GIA must be removed from the observations. The deformation of the solid Earth can be detected on the surface by GNSS data on rock outcrops adjacent to the ice sheets (Scheinert *et al.* 2021, this volume). Many of such observations are available in Greenland, for example (Bevis *et al.* 2012), but observations in Antarctica are much more spread out due to the harsh terrain and because most of the bedrock is covered in ice. Therefore, to obtain spatial patterns of surface deformation, as well as to correct other relevant climate indicators for GIA, numerical simulations are used together with available observations (e.g. Whitehouse *et al.* 2019). With the increasing coverage of geodetic measurements, inversion techniques can exploit different sensitivities to changes in ice, snow and the solid Earth in order to separate out the measured signals (see Martín-Español *et al.* 2016*a*; Scheinert *et al.* 2021, this volume).

The GIA process is also an interesting topic of study in itself. The growth and decay of an ice sheet can be seen as a large deformation experiment. The response of the Earth's surface is governed by the viscosity of the underlying mantle, so measuring the GIA can be seen as a way to measure viscosity at depth. As viscosity is the parameter that controls the speed of motion in the Earth's mantle, which drives plate tectonics, constraining viscosity is an important contribution of GIA research. However, since viscosity affects several processes in the Earth, such as mantle convection (e.g. Bredow *et al.* 2022, this volume). GIA studies are not the only way to infer the viscosity of the Earth's interior. GIA research complements other methods for estimating viscosity: for example, through seismic models (e.g. Lloyd *et al.* 2020; Wiens *et al.* 2021, this volume) and laboratory experiments on mantle rocks (Hirth and Kohlstedt 2004), combined with information on rock composition and local mantle conditions derived from xenoliths (e.g. Martin 2021, this volume). How viscosity is derived for use in GIA models is described in Ivins *et al.* (2021, this volume).

This section presents methods for modelling GIA, discusses the main inputs and results of this modelling, and the observational constraints. It starts with a brief general history of GIA in general, after which the state of the art on GIA modelling in Antarctica is presented. In terms of data, the focus is on relative sea level (RSL: the difference between the surface of the sea and the ocean bottom), as the geodetic data are already described in Scheinert *et al.* (2021, this volume). Concerning numerical models, attention is paid to the description of the models themselves and their inputs, with a focus on ice thickness, as rheology is covered in Ivins *et al.* (2021, this volume). The focus is on the last glacial cycle because this influences present-day geodetic observations and more observations of the GIA process are available for this period. GIA projections for the Antarctic Ice Sheet are briefly addressed and the section concludes with pointers for future research.

Brief history of GIA research

What follows is a brief summary of the history of the concept of GIA up to the point that numerical models were used extensively from the 1980s. A more extensive history can be found in Ekman (1991), Steffen and Wu (2011) and Whitehouse (2018). Historically, the concept of GIA is associated with Fennoscandia, specifically a small Swedish village on an island in the Baltic Sea, where in 1731 Anders Celsius was invited to explain why a group of rocks in the coastal area was apparently slowly rising above the level of the sea (Ekman 2013). Even though Celsius and his contemporaries did not realize it at the time, they were observing land uplift and a sea-level readjustment caused by deglaciation since the LGM (*c.* 20 kyr ago). Given the strategic role of these rocks, which had been used for hunting seals for centuries, empirical records of their height with respect to sea level had been kept for generations, allowing the phenomenon to be tracked that would otherwise have been difficult to notice in one life time. All the important elements of GIA were already present: the uplift of the Earth's surface, the role of RSL as a reference for the Earth's deformation and the speed (or, rather, the slowness) of the phenomenon.

Celsius was able to compute the uplift rate of the rock; however, he was not able to provide the correct explanation, which was suggested first in 1865 by Thomas Jamieson who argued that 'the enormous weight of ice thrown upon the land may have something to do with this (land level) depression' (Jamieson 1865, p. 178). Until the pioneering work of Haskell (1935), there had been no attempt at quantitative modelling. Haskell used a simplified model that neglected the crust but considered a viscous layer underlain by a rigid layer on which the load was applied. To constrain his model, he used records of past changes in RSL. Assuming a certain thickness for the upper layer, he estimated the viscosity of this viscous layer to be around 10^{21} Pa s. The number, although based on a model that is incomplete, is remarkably close to the modern estimates of the average viscosity for the upper mantle (Mitrovica 1996). A viscosity of this magnitude translates into a characteristic relaxation timescale of thousands of years.

The success of Jamieson's idea of a vertical viscous response of the Earth to deglaciation was one of the main arguments used by Wegener in his book *The Origin of Continents and Oceans* (first published in 1915 in German; Wegener 1915) in favour of his new hypothesis of continental drift. He argued that if vertical viscosity-regulated motions could occur, it could also be possible that horizontal motions could be sustained. Thus, the idea of GIA predates, and even contributed to, the idea of continental drift.

New and more reliable methods to date sedimentary changes (palynology and, later, carbon dating) substantially improved and significantly expanded the sea-level records, stimulating the development of new GIA models. In the 1970s, the first spherically symmetrical, self-gravitating, models were developed (Peltier 1974; Cathles 1975). Spherically symmetrical means that the Earth model consists of concentric layers with constant properties, while self-gravity refers to the inclusion in the model of changes in gravity due to deformation. This can be considered the beginning of modern GIA modelling. A lot of effort went into reproducing the increasingly precise sea-level records with ice-history reconstructions and inferring the Earth's viscoelastic properties for distinct

layers as opposed to a single average value. This required a detailed understanding of the relation between the spatial characteristics of the load and the sensitivity of the response of the different components of the model such as the lithosphere thickness and the viscosity profile.

Parallel to the studies on the solid Earth, ideas developed on the adjustment of sea level, the concept of 'eustasy'. Edward Suess (1888) described the idea that sea level is at a minimum during a glaciation when water from the oceans gets stored on land in the form of ice, and that it then reaches a maximum in the interglacial periods when the ice sheets retreat. However, this concept results in a uniform sea-level variation during the glacial oscillations, treating the ocean basin as a giant bathtub with extremely steep boundaries between water and land that is filled or depleted as needed. This is in contradiction with what records of sea level show. Palaeoreconstructions of sea level based on geological observations and debris dating that cover several millennia show a much more varied behaviour: sea-level records at the coasts close to the regions covered in ice at the LGM consistently show a sea-level fall in Fennoscandia and North America (Walcott 1972). Clearly, there is another process acting. The analogy of the bathtub fails because it neglects gravity, which dominates on a global scale. Moving large masses around changes the gravity and equipotential surfaces that determine sea level at rest. The inclusion of gravitational forces explains how the melting of a large ice sheet reduces gravity in a region around the shrinking ice sheet, so that the equipotential surface is lowered and a local sea-level decrease is obtained (Farrell and Clark 1976; Clark *et al.* 1978). Changes in the gravity field and changes in sea level cause deformation of the Earth, and are important to include in GIA models.

To get an idea of the magnitude of deformation, we quantify the GIA process in some key areas. Huge continental ice sheets of more than 3 km in thickness covered Canada, northwestern Europe (Fennoscandia) and West Antarctica at the LGM when they started melting *c.* 20 kyr ago. Melting was essentially completed 7 kyr ago and resulted in a net rise of the mean sea level over the global ocean of about 130 m between LGM and present day (Clark and Tarasov 2014). This net increase in water is called a eustatic sea-level rise and it reached a rate of 40 mm a^{-1} during the deglaciation period (Lambeck *et al.* 2014). Due to the lag in Earth deformation having a characteristic timescale of thousands of years, the solid Earth surface in former ice-covered regions is currently uplifting by up to 10 mm a^{-1}. Just beyond the ice sheets, forebulges emerged during the growth of former ice sheets (see a schematic representation in Fig. 1), which currently subside at a rate of several millimetres per year, as detected by GNSS instruments (e.g. Schumacher *et al.* 2018). Thus, the bedrock deformation under the present-day ice sheets differs per region, depending on the historical and current loading and unloading of ice.

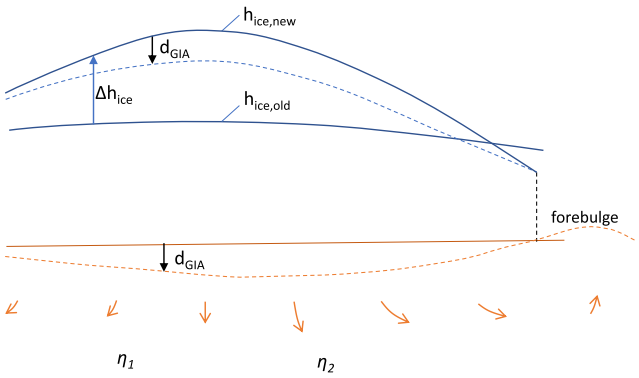

Fig. 1. Schematic representation of GIA following an increase in ice thickness of an ice sheet resting on a bedrock that has two different viscosities. The ice thickness increases by Δh_{ice}. As a result of this increase and past increases in ice thickness, the bedrock deforms by d_{GIA} with a forebulge forming outside the area of ice increase. Because viscosity η_2 is assumed to be smaller than η_1, deformation is larger under the right half of the ice sheet in a given time.

GIA physics simplified

When a load is placed on the Earth, after initial elastic displacement, pressure is distributed into the mantle, which deforms in a way that can be compared to deformation of memory foam or a sponge after pressing it: a slow readjustment to equilibrium controlled by the dynamic viscosity parameter, η, that is usually used for viscous flow (Fig. 1). Measurable deformation some time after the change in load occurs if the viscosity is low enough for rocks to creep on timescales of a glacial cycle or shorter. The numerical models used to compute GIA and post-seismic relaxation are generally viscoelastic, meaning that they include a viscous component as well as instantaneous elastic changes in deformation and in the gravitational field (and, therefore, in sea level). The Earth's interior, down to the fluid outer core, can be considered viscoelastic but the top layer is essentially elastic and is termed the lithosphere (not shown separately in Fig. 1). The flexural rigidity of the lithosphere acts as a dampening filter for both the forcing and the consequent deformation. The thinner the lithosphere, the more spatially concentrated is the deformation induced on the mantle; the thicker the lithosphere, the more distributed is the deformation. This can be used to infer the thickness of the lithosphere when the load's spatial and temporal histories are known. Finally, brittle deformation also occurs within the lithosphere, causing fractures under stress associated with surface loading, but this plays a smaller role in relieving overall stresses. This can be understood from the observation that GIA-induced earthquakes have a small effect on nearby faults (Brandes *et al.* 2015).

The subsidence below a thickened ice sheet must be compensated by uplift elsewhere because although the Earth is compressible, its volume does not change significantly. The basic shape of a GIA pattern is a concentric pattern of deformation, the so-called footprint of the ice sheet, with uplift in a band around the ice load – the forebulge (Fig. 1). Upon melting of the ice sheets, meltwater flows into the oceans and the overall mass distribution on the Earth's surface changes. This results in changes in the gravitational pull and a sea-level fall near the ice sheet that were mentioned in the previous subsection. The spatial pattern of sea-level change that results from ice melt has been labelled 'sea-level fingerprint' (Mitrovica *et al.* 2009), and includes gravitational effects and elastic deformation due to ice melt. In addition, the meltwater acts as a load that is redistributed across the globe, and which deforms the ocean basins. This leads to continental levering, which is the subsidence of the ocean floor and a corresponding uplift of the neighbouring continent as a result of the addition of meltwater (Walcott 1972; Mitrovica and Milne 2002). Also relevant to the sea-level change is the concept of ocean syphoning, where water flows from equatorial regions towards forebulges that are subsiding below the ocean, especially around Canada and Antarctica (Mitrovica and Peltier 1991).

Further improvements in sea-level modelling account for shifting land–ocean boundaries (Johnston 1993; Peltier 1994) and grounded ice that can become floating as sea level rises (e.g. Milne *et al.* 1999). Finally, the change in ice load and deformation of the Earth affect the Earth's moment

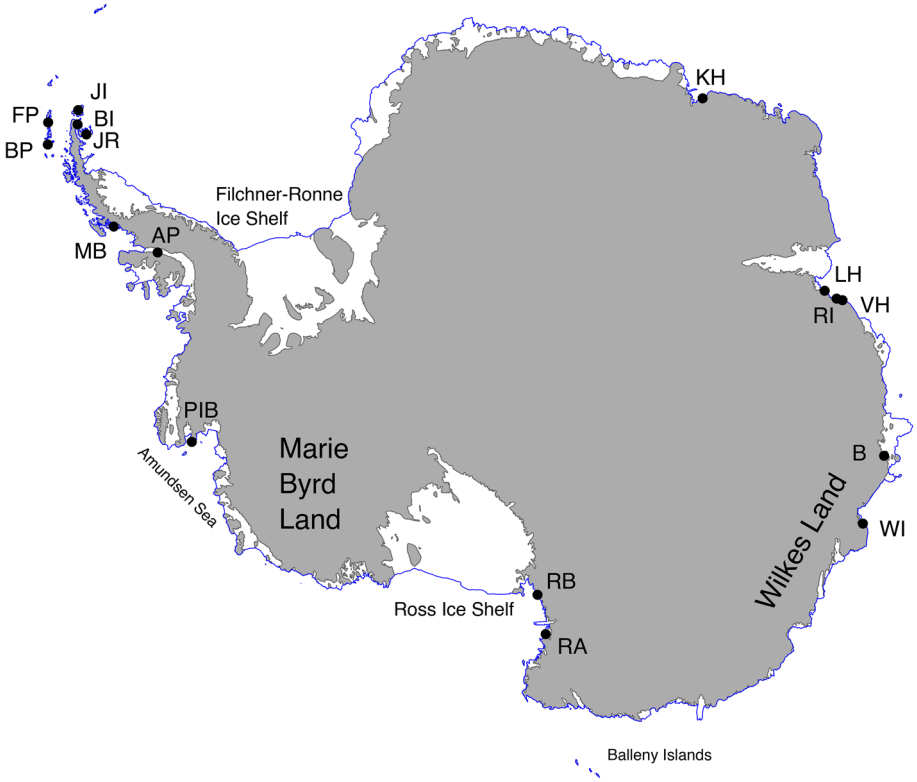

Fig. 2. Relative sea-level data in Antarctica compiled in Whitehouse *et al.* (2012*a*) (largely based on Bassett *et al.* 2007) and sites from Okuno and Miura (2013). Locations going along the coastline clockwise starting at KH: KH, Kizahasi Hama; LH, Larsemann Hills; RI, Rauer Islands; VH, Vestfold Hills; B, Bunger; WI, Windmill Island; RA, Ross A (Terra Nova Bay); RB, Ross B (Cape Roberts); PIB, Pine Island Bay; AP, Ablation Point; MB, Marguerite Bay; BP, Byers Peninsula; FP, Fildes Peninsula; JI, Joinville Island; BI, Beak Island; JR, James Ross. The 200 largest grounded regions are patched grey, and Antarctica's coast (including ice shelves) is shown in blue. These are plotted with MATLAB routines from Antmap (Greene *et al.* 2017) based on Bedmap2 (Fretwell *et al.* 2013).

of inertia, which changes the direction and magnitude of the rotational vector of the Earth. This in turn changes the rotational potential, which induces deformation of the solid Earth as well as changes in sea level (Bills and James 1996; Milne and Mitrovica 1998).

Considering the discussion of GIA above, it is clear why records of sea level at different locations on the globe can be used to gain knowledge on the history of deglaciation and on the Earth's physical properties. In the following subsection, we discuss observations available in Antarctica, including sea-level records.

GIA observations in Antarctica

Constraints on GIA are much more sparse in Antarctica than in other continents but the quantity and the quality has been steadily improving, so that a robust picture appears of some aspects of GIA in Antarctica. In this subsection, we discuss palaeosea-level data; geodetic data are reviewed in Scheinert *et al.* (2021, this volume). In addition to these two types of data, there are a few other manifestations of the GIA process that could be considered as observable. Post-glacial rebound is hypothesized to have contributed to the 1988 Antarctic earthquake south of the Balleny Islands (see their location in Fig. 2) (Tsuboi *et al.* 2000). Seismic events in the Ellsworth Mountains are thought to be related to ongoing GIA-induced stress, acting on pre-existing structural weaknesses (Lucas *et al.* 2021). Stress orientation obtained from boreholes indicates that significant GIA stress is present that could have triggered other earthquakes (Ivins *et al.* 2003). Glacial-induced earthquakes have also been suggested as contributing to sediment slides in the Miocene in the Western Wilkes Land margin (Donda *et al.* 2008). These hypotheses are interesting to explore in future modelling but as of yet do not yield useful constraints on GIA models.

Sea-level indicators. Information on sea level can come from the dating of organic material such as shells and seaweed in raised beaches. A clear raised beach is not always visible as the land rise and corresponding sea-level change happens gradually. Some findings indicate a minimum height for sea level, such as shells: sea level must have been higher than the location at which they are deposited (e.g. Bentley *et al.* 2005). Some findings represent a maximum sea level as they are deposited subaerially, such as seal hairs and penguin droppings (Bassett *et al.* 2007). Sometimes sea-level tilt can be derived, which provides a stronger constraint on spatial sea-level changes (Konfal *et al.* 2013).

The most accurate data are taken from so-called isolation basins. When land is rising, bodies of water that lose their connection to the sea transition from marine to lacustrine. This transition is recorded within the sediment deposited in these water bodies, and can be detected in sediment core studies and dated. The reverse can also occur: a transition from lacustrine to marine sediments indicates a sea-level rise.

A number of sea-level indicator data in Antarctica has been reported in recent literature; their location is shown in Figure 2. Bassett *et al.* (2007) compiled data from eight locations; their location is shown in Figure 2, which was extended in Whitehouse *et al.* (2012*a*) to 14 sites that were also used by Argus *et al.* (2014). Okuno and Miura (2013) used a subset of these data and included an extra site in East Antarctica (Bunger). Furthermore, raised beaches in the northern part of the Antarctic Peninsula have been dated to the late Holocene, indicating increasing sea-level fall during that time (Simms *et al.* 2018). A reconstruction in Joinville Island at the tip of the Antarctic Peninsula shows a sea-level fall in the last 3 kyr, with significant changes in rates (Zurbuchen and Simms 2019). Records in East Antarctica have been extended by Hodgson *et al.* (2016) and Verleyen *et al.* (2017), with the latter pointing out the possibility of neotectonics contributing to vertical deformation.

The amount of sea-level data is sparse, and there are no data available between the LGM and 12 ka before present (BP). However, in several locations beach deposits and lake and sea sediments can be used to infer sea level before the LGM (e.g. Nakada *et al.* 2000). They indicate a sea level

close to present, which could only have been achieved with excessive ice (due to the self-gravity of the ice sheet), that would place the glacial maximum well before 20 ka (Ishiwa *et al.* 2021).

Interpretation of the GIA observations require numerical models to compute uplift rates and gravity changes for a given Earth model and ice-sheet thickness history, which can then be compared to the observations. Results of numerical GIA models are discussed in the following subsection.

Numerical models and results

The earliest GIA models solved the differential equations describing the physical phenomena involved, starting with the conservation of momentum and mass (Cathles 1975). The traditional way of solving them is by means of the normal mode method (Peltier 1974; Wu and Peltier 1982). This method is suitable for a layered Earth with radially varying viscoelastic parameters. The normal mode method succeeds in computing the response for a spherical body with concentric layers with constant parameters (we will refer to this as a 1D model), where the response is the change in deformation and the change in gravity. For each layer, the elastic parameters (density and Young's modulus) and viscosity need to be specified. For ice-dynamics models, the GIA component is often simulated by a model that is conceptually simpler than the normal mode method, the so-called elastic lithosphere and relaxing asthenosphere (ELRA) model, which will be addressed in the 'Coupling of ice to solid Earth: feedbacks and processes' subsection later in this section. The asthenosphere is the upper part of the upper mantle below the lithosphere. For the ELRA model, parameters are also constant for the two layers involved.

The normal mode theory assumes linear viscoelasticity, which means that stress is proportional to strain at a given time and the response to different stresses can be summed (Findley *et al.* 1976). Peltier (1974) and Wu and Peltier (1982), along with many others following their methodology, assume a Maxwell rheology (e.g. see Sabadini *et al.* 2016), which is a particular form of linear viscoelastic rheology where the elastic deformation occurs first upon the application of a force, which can be the increase in weight of the ice sheet, after which viscous deformation takes over. Other linear viscoelastic rheologies have been employed in GIA models: for example, the Burger's rheology, which uses a separate viscosity for the short-term initial and the long-term steady-state responses (Yuen and Peltier 1982; Sabadini *et al.* 1985). This rheology is commonly used in post-seismic deformation (see 'Conclusions and future work' later in this chapter). It has not been used widely to explain GIA observations since the first studies in the 1980s but it has received more attention recently (Caron *et al.* 2017; Ivins *et al.* 2020), not least because the behaviour in deformation experiments points towards Burger's rheology (Faul and Jackson 2015). Nonlinear rheology, in which the strain rate depends non-linearly on stress, has also been included early on in GIA modelling (e.g. Nakada 1983; Wu 1992), with more recent use in GIA models informed by laboratory experiments on mantle rocks (e.g. van der Wal *et al.* 2013).

Model results produced by the normal mode method can explain GIA observations to a large extent for a global average viscosity profile (e.g. Peltier 2004; Lambeck *et al.* 2014; Lau *et al.* 2016), although studies do not all agree on the same radial viscosity profile, partly because of non-uniqueness in the inversion: different viscosity profiles can explain the same subset of observations to within the noise level (Paulson *et al.* 2007). Viscosity in the real Earth can vary by orders of magnitude but the normal mode method can still be used for applications in regions where viscosity variations underneath and near the ice sheet are small enough that viscosity can be approximated by an average value that varies with depth only.

For several regions, including Antarctica, viscosity cannot be assumed to be constant beneath the ice-covered region, and the viscosity, along with other Earth material properties in the model, needs to change with latitude and longitude. To model the effect of such lateral variations in viscosity, numerical methods are generally applied in which the Earth is discretized into small elements, finite elements or finite volumes. Global spherical Earth models that can incorporate lateral variations in viscoelastic parameters have been developed since the 2000s (Martinec 2000; Zhong *et al.* 2003; Wu 2004; Latychev *et al.* 2005). These models are sometimes referred to as 3D GIA models, where 3D refers to the variations in the Earth model input rather than the domain of the model itself. Most knowledge on GIA still comes from global 1D models as these have been around longer, and because 3D models have a long computation time and a potentially large number of degrees of freedom requiring additional constraints.

The largest uncertainty in GIA models stems from the unknown ice thickness through time. For several regions, ice sheets have left marks in the landscape from which the ice extent can be contoured and dated. However, in Antarctica, the ice sheet still covers most of the land and changes in the thickness of the ice sheet have left little indication on the landscape, unless particular glaciers were confined to a mountain valley that show the erosional limits (trimlines: Denton *et al.* 1992; Bentley and Anderson 1998) or there is other geological evidence: for example, from glacial and post-glacial deposits (e.g. Brook *et al.* 1993; Mackintosh *et al.* 2014) or glaciovolcanology (Smellie *et al.* 2009, 2011). An overview of studies on the large-scale changes in the Antarctic Ice Sheet since the LGM is given in the following subsection.

For the GIA-based method of inferring ice-sheet history, a forward GIA model is used that assumes a certain viscosity profile. However, the mantle viscosity is often derived from GIA studies that assume a certain ice history. This circularity is reduced by the different data available and the different sensitivities they have to the input Earth model parameters. For example, depending on the spatial scale of the load, the depth at which the mantle responds the strongest changes: smaller ice sheets, such as in Scotland, affected a shallower part of the mantle, while the largest ice sheets, such as the Laurentide Ice Sheet, excited a response in the lower mantle. This characteristic can therefore be used to employ observations around different ice sheets to constrain viscosity at different depths of the mantle. This qualitative idea has been confirmed by computing 'sensitivity kernels' from numerical models (Peltier 1976; Wu 2006; Lau *et al.* 2016) that show which depth of the mantle has the most impact on a certain observable. A sensitivity kernel can be computed with a forward GIA model. A small change in the viscosity in a small sublayer is applied and the change in the observable is computed, all with respect to a certain reference viscosity profile. By doing this for many sublayers, a plot can be created of the effect in the observable v. the depth at which the viscosity change is applied. An example for the Scandinavian Ice Sheet is shown in Figure 3. In this case, the observable is the present-day change in gravity but the curves would be similar for present-day uplift rate. Note that the magnitude itself is not relevant as it scales with the magnitude in the viscosity change but the relative magnitude is interesting. The sign is positive in the figure, meaning that the change in viscosity increases the gravity rate. However, a negative sign could also be achieved because both a viscosity that becomes very low and a viscosity that becomes very high will reduce gravity and uplift rates. The sensitivity with depth is directly dependent on the viscosity: for a profile with higher viscosity in

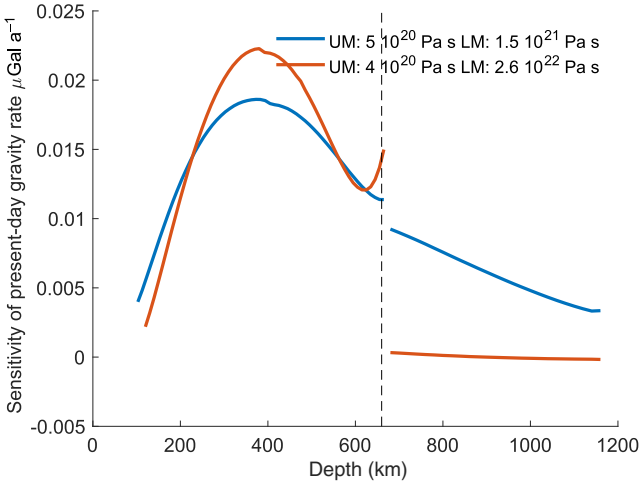

Fig. 3. Sensitivity of the present-day gravity rate in the centre of the Scandinavian ice sheet to viscosity at depth for two viscosity profiles. UM, upper mantle, above 670 km; LM, lower mantle, between 670 km and the core. The ice-sheet model used is ICE-5Gv1.2 (Peltier 2004). Source: Reproduced from van der Wal *et al.* (2011).

the lower mantle (orange line), more of the sensitivity is concentrated in the upper mantle. For Antarctica, the change in ice-sheet thickness since LGM in West Antarctica is similar to the thickness of the Scandinavian Ice Sheet but with a smaller spatial extent. Therefore, the sensitivity is expected to be concentrated at a shallower layer compared to what is shown in the figure.

A further reduction in the circularity of the problem is possible by recognizing that relaxation after the ice has disappeared mostly depends on the viscosity and not on the ice history (Wieczerkowski *et al.* 1999). Furthermore, combining and integrating sea-level records with GNSS measurements of uplift rate and gravity variation measurements from GRACE and GRACE-FO (GRACE Follow-On) satellite measurements reduces the uncertainty, although unique inversion for viscosity in three layers or more is challenging, even with a combination of these data (Paulson *et al.* 2007).

Despite the limitations, the GIA approach allows an estimation of Earth properties of the lithosphere and mantle that complements information coming from other geological, geophysical and geodynamic studies. Global GIA models predict RSL and other observations from all over the world, taking into account the global effect of the water redistribution by computing the sea-level change that is consistent with the loading and solid Earth deformation. Modern analyses indicate that the global average value for upper-mantle viscosity lies close to the value suggested by Haskell in 1935 (Mitrovica 1996) as stated in the earlier subsection on 'Brief history of GIA research'. A refinement of this result indicates that viscosity increases from the upper to the lower mantle by a factor of 2–3 (e.g. Peltier 2004) or more (e.g. Kaufmann and Lambeck 2002). The characteristics of the GIA process are such that both the low-viscosity and the high-viscosity solutions are allowed by the sea-level data (Lambeck *et al.* 2014) but the ambiguity in the lower-mantle viscosity can be reduced by including constraints on the Antarctic ice volume (Caron *et al.* 2017).

The estimates discussed above represent an average value for viscosity. They will provide incorrect predictions of RSL change and modern uplift rates in areas where the actual viscosity structure greatly deviates from the global average, such as in West Antarctica. The solid Earth's internal properties and Earth's loading history are interdependent in GIA inversions and both are unknown at a fine scale even if a global picture emerges. All of these problems exist in Antarctic GIA studies but steady progress with increased measurements and model refinements has led to GIA results for Antarctica that are gaining acceptance.

In 3D GIA models, the larger number of degrees of freedom combined with a longer computation time prohibit simulating a large parameter space. For this reason, uncertainty in 3D model predictions is not well quantified. However, 3D GIA models provide higher accuracy over 1D models for several applications. Some key sensitivities of GIA models can be summarized to facilitate interpretation of model results. First, the bedrock response at a certain location depends on the ice-sheet forcing in the surrounding area. The stress is transported from the area of loading downwards into the mantle but also outwards where it also deforms the surface. The observed response is a function of viscosity along this stress path (Paulson *et al.* 2005). As stress is largest beneath the load, viscosity beneath the load has a large control on the bedrock response but viscosity outside the loading area is also relevant. For example, near the edge of the ice sheet, the uplift rate is most sensitive to the local viscosity as opposed to the viscosity beneath the load (Wu 2006). In fact, this sensitivity is as strong as the sensitivity of the uplift rate to the viscosity in the centre of the ice sheet. RSL data outside the ice cap have an even stronger sensitivity to the viscosity outside the ice sheet; sensitivity to viscosity at a certain depth can have an opposite sign between two locations near the observation point (Crawford *et al.* 2018). This shows that RSL data have more resolving power inside the Earth than the uplift rate data, which demonstrates the importance of RSL data for GIA inversions. The RSL data was discussed in an earlier subsection.

Ice-sheet history in Antarctica

Applying a forward GIA model requires the ice thickness through time to be known. To reconstruct such a history, glacial geological constraints, ice-dynamics modelling and GIA observations are used, or a combination of these (e.g. Bentley 1999; Briggs and Tarasov 2013; Siegert *et al.* 2022). In the case of ice dynamics, ice-sheet behaviour is simulated using climatic conditions as input (e.g. Huybrechts 2002). In a GIA-based scheme, ice thickness is adjusted until a good fit is obtained with palaeo sea-level records, possibly including geodetic data (e.g. Peltier 2004). Several approaches lie in between: a simplified ice model with a regional tuning parameter (Lambeck *et al.* 2017; Gowan *et al.* 2021) or averages of an ensemble of ice-physics-based realizations can be employed (Tarasov *et al.* 2012).

Geological inferences of ice thickness. Comprehensive geological and ice-core data have become available for the deglaciation since the LGM. The extent of the ice sheet can be derived from ice-marginal features such as moraines, subglacial features and glacial deposits, which can be dated using different techniques (e.g. Whitehouse *et al.* 2012*a*; Siegert *et al.* 2022). An important dating technique is cosmogenic nuclide surface exposure dating. Nuclides form in rocks as a result of bombardment by cosmic rays. The longer a rock is exposed, the more nuclides it will contain. Therefore, counting the nuclides gives an indication of the time that the rock has been exposed, which can pinpoint the formation of a moraine or other features (Davis 2020). The technique, however, is affected by GIA itself, as the elevation of the sample affects nuclide production (e.g. Jones *et al.* 2019).

A second dating technique is optically stimulated luminescence dating, which measures the remaining electrons created from naturally present radioactive material after the electrons are 'reset' by exposure to sunlight before ice crystals are deposited. Where organic material is present, carbon dating

can be used: for example, organic material in sediments or of animal remains at raised beaches. The latter usually provides a minimum age: whenever animals were present there was no ice. However, carbon dating is affected by natural variations in the background rate and, therefore, the ages have to be calibrated to calendar ages before they can be compared with model predictions.

Other data include mapping of grounding lines by seismic reflection profiles and sonar (Whitehouse *et al.* 2012*a*), and detection of grounding-line retreat in the transition of sediments (Briggs and Tarasov 2013). Such data are sparse in East Antarctica (Arndt *et al.* 2013) but exposure dating of glacial features has been performed for a number of locations on the coast of East Antarctica (Mackintosh *et al.* 2014). In the interior, constraints are more difficult to obtain. The isotope distribution in ice cores can be a proxy for the ice-accumulation rate, from which changes in ice thickness can be obtained (e.g. Parrenin *et al.* 2007). This requires an ice-flow model but also an accurate model for bedrock elevation and its changes (e.g. Siddall *et al.* 2012).

Finally, glaciovolcanism offers insights into ice-sheet parameters, such as age, thickness and surface elevation (Smellie 2018). The contact of lava with ice produces meltwater when the volcanic cone reaches the bottom of the ice sheet. The interaction of meltwater and lava produces a recognizable stratigraphic unit. Therefore, the thickness of the layer thus produced approximates to the thickness of the prevailing ice sheet. The elevation of the layer can also indicate the thermal regime, whether ice is cold or wet based (e.g. Smellie *et al.* 2011). The advantage of glaciovolcanic evidence is that volcanic deposits are thick and are resistant to erosion but the time resolution can be low as it depends on eruption frequency. Applications in Antarctic include the Antarctic Peninsula Ice Sheet in the Pliocene (Smellie *et al.* 2009; Davies *et al.* 2012), and the thermal regime of the East Antarctic Ice Sheet between 12 Ma and present (Smellie *et al.* 2011). The compilation by the RAISED Consortium in 2014 provided time-slice maps of grounding-line position and ice-sheet thickness at 5 kyr intervals (Bentley *et al*. 2014; see also Siegert *et al.* 2022). The results agreed with earlier findings of a total volume of Antarctic ice loss since the LGM of below 10 m sea-level equivalent (SLE). The amount of retreat varies across Antarctica, with the largest retreat found in the marine-based sector of the Ross and Filchner–Ronne ice shelves (for their location see Fig. 2). The timing of retreat also varied, from early retreat in the Antarctic Peninsula and the Amundsen Sea sector to late retreat in Marie Byrd Land (for the locations see Fig. 2). However, ice also advanced in the late Holocene (e.g. in the Antarctic Peninsula: Simms *et al.* 2021), as possibility already hinted at in Hollin (1962). In East Antarctica, ice extended to the shelf at the LGM but was probably thinner in the interior (Mackintosh *et al.* 2014). Recently, the role of ocean–ice interaction has received more attention. This interaction could provide a means for parts of East Antarctica to be susceptible to instability caused by the ocean 'eating' into an ice sheet on deepening topography (Schoof 2007; Kawamata *et al.* 2020).

Ice-sheet dynamics. To recreate an ice sheet, knowledge of the dynamics of an ice sheet is helpful but an ice sheet is subject to many forces and interfaces that are difficult to take into account. In particular, the interactions of an ice sheet and shelves with bedrock in subglacial water transport and with the ocean are crucial but complex, and are an active area of research (Siegert and Golledge 2022). Therefore, a unique representation of the ice sheet through time cannot come from ice dynamics alone. Proxies for total ice volume and evidence of the maximum ice extent can help to limit the range of ice-sheet realizations. However, at the same time it is difficult to create a model of ice dynamics that matches available data (Briggs and Tarasov 2013). Moreover, high spatial resolution in the models and in the input data such as topography is required to represent ice flow accurately, which is not yet feasible (Colleoni *et al.* 2018). What ice-sheet-dynamics models can provide is a shape for the ice sheet that is physically more realistic than ice sheets that are tuned to sea-level data or ice-extent data only. They can also provide uncertainty estimates based on physical parameters (e.g. Albrecht *et al.* 2020*b*).

A widely used Antarctic Ice Sheet reconstruction is CLIMAP (Hughes 1981; Stuiver *et al.* 1981), on which several GIA models were based (Nakiboglu *et al.* 1983; Wu and Peltier 1983). It consists of a 2D ice model with a basal shear parameter – the main degree of freedom. The total volume of ice melted since the LGM amounted to 24 m SLE. The Antarctic-wide reconstruction by Huybrechts (1990) showed in more detail that the Antarctic Ice Sheet behaved similar in time to the northern hemisphere ice sheets, and that most of the ice loss occurred on West Antarctica. Denton and Hughes (2002) obtained a value of 14 m SLE for Antarctic Ice Sheet loss since the LGM. Early models were not yet able to reproduce the processes that act on the grounding line such as damage, and calving and basal melting (Pattyn *et al.* 2017). These processes are very relevant for the post-LGM ice history in Antarctica as fast-flowing glaciers in response to ocean forcing can drain large glacier catchments (Golledge *et al.* 2012). More recent models do not result in an ice sheet extending to the continental shelf; they indicate thinner ice sheets with a smaller contribution to the period of fast sea-level rise known as Meltwater Pulse 1A, which occurred *c.* 14 kyr ago (Albrecht *et al.* 2020*b*).

Figure 4a shows the time history of the Antarctic Ice Sheet volume since the LGM for several recent ice models. Figure 4b indicates the total contribution of the Antarctic Ice Sheet to global sea level since the LGM (based on fig. 11 of Albrecht *et al.* 2020*b*). Note that some studies used volume of grounded ice above flotation (VAF), rather than total volume of grounded ice, which gives a smaller SLE. Ice thickness above flotation is what contributes to the loading of the Earth's surface (see Goelzer *et al.* 2020). It can be seen that studies which simulate the dynamic behaviour of the Antarctic Ice Sheet yield the largest variations. Variations also stem from the timing of the LGM being unclear (Bentley *et al.* 2014), varying, for example, from 25 ka BP (Briggs *et al.* 2014) to around 16 ka BP (Maris *et al.* 2014), although most studies assume little decline in that period. In general, ice-sheet melting and retreat is not synchronous across Antarctica (Bentley *et al*. 2014). Some sections, such as the Antarctic Peninsula and Amundsen Sea sector, responded faster to temperature increase than others such as the Ross and Filchner Ronne ice shelves and Marie Byrd Land. There is also evidence for a minimum ice extent several thousands of years BP, and growth thereafter (e.g. Siegert *et al.* 2022). Such behaviour will by itself lead to subsidence, which complicates the interpretation of GIA observations.

GIA-based ice-sheet reconstruction. Ice-sheet thickness determines land uplift and the shape of the sea surface (see the earlier subsection on 'GIA physics simplified'), and, therefore, sea-level estimates can be used to infer ice thickness. The first constraint is that the total volume of loss of land-based ice should match the global mean sea-level rise. A further refinement in locating past land ice is possible by combining sea-level indicators located near the centre and edges of the former ice sheet and in the far field. This requires a GIA solver that can provide predictions of sea-level change. When such a solver is used, the ice inferences are no longer independent of the

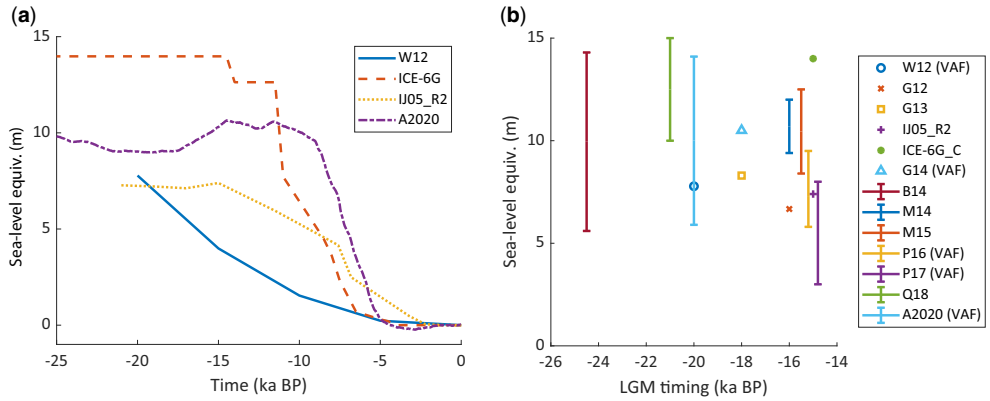

Fig. 4. (**a**) Contribution of the melting of the Antarctic Ice Sheet to global sea-level rise since the LGM for different ice models or studies of LGM ice cover. W12, Whitehouse *et al.* (2012*a*); ICE-6G, Argus *et al.* 2014; IJ05_R2, Ivins *et al.* 2013; A2020, Albrecht 2019; Albrecht *et al.* 2020*b*). The change in ice thickness is converted to volume of water using ice and ocean densities of 917 and 1000 kg m^{-3} and then dividing by the present-day ocean area of 361 × 10^6 km^2 to obtain SLE. For Whitehouse *et al.* (2012*a*), the output from the Glimmer ice-sheet model at 5 kyr intervals is used, from which the area above flotation is calculated using topography consistent with the ice-sheet model. (**b**) Total contribution of the melting of the Antarctic Ice Sheet to global sea-level rise since the LGM, as well as the LGM timing for selected studies. For some studies a range is provided, for others only a single number is available. Numbers are taken from Albrecht *et al.* (2020*b*), except where authors reported a different value or range in the original paper. W12, Whitehouse *et al.* (2012*a*); G12, Golledge *et al.* (2012); G13, Golledge *et al.* (2013); IJ05_R2, Ivins *et al.* 2013; ICE6G_C, Argus *et al.* (2014); G14, Golledge *et al.* (2014); B14, Briggs *et al.* (2014); M14, Maris *et al.* (2014); M15, Maris *et al.* (2015); P16, Pollard *et al.* (2016); P17, Pollard *et al.* (2017); Q18, Quiquet *et al.* (2018); A20, Albrecht *et al.* (2020*b*). VAF indicates that grounded ice above flotation is used to compute the sea-level contribution.

assumed mantle viscosity or other rheological parameters. A further limiting factor is that sea-level indicators are only found in Antarctica in select places near the edge of some of the ice sheets or shelves (see the earlier subsection on 'GIA observations in Antarctica'). Therefore, due to the lack of local constraints, in global GIA models until 2010 Antarctica has mostly been used to match the total sea-level change during the deglaciation (e.g. Lambeck *et al.* 2000). Wu and Peltier (1983) used an ice sheet by Clark and Lingle (1979) in their ICE-2 global reconstruction model; the timing was later adjusted by Peltier (1988). Nakiboglu *et al.* (1983) took estimates of the total melt volume and created a more detailed distribution of ice over the Weddell and Ross seas. The CLIMAP model was revised downwards in terms of volume by Nakada *et al.* (2000), whose range of 6–17 m SLE is closer to recent estimates. James and Ivins (1998) provided simulations of the uplift rate that could be tested by GPS data, which became available in the years thereafter (see Scheinert *et al.* 2021, this volume). Since then, reconstructions have relied more upon ice extent, thickness change, ice-dynamics estimates (Whitehouse *et al.* 2012*a*; Ivins *et al.* 2013; Argus *et al.* 2014) and GPS uplift rates (Argus *et al.* 2014).

Ice sheet histories used in GIA models. In the following we discuss ice-sheet histories that are widely used in GIA models, especially those that are used to correct GRACE measurements of mass change: W12 (Whitehouse *et al.* 2012*a*), IJ05-R2 (Ivins *et al.* 2013) and ICE-6G_C (Argus *et al.* 2014). We discuss the model of Albrecht *et al.* (2020*b*) as a recent example of a ice-dynamics model, specifically the best scoring simulation as shown in figure 15 of that paper.

Whitehouse *et al.* (2012*a*) assembled all the pertinent glacial-geological data and used a shallow ice numerical code to examine a spectrum of possible ice-change scenarios. Ice-thickness changes between 20 ka BP and the present as provided by this model are plotted in Figure 5a. The greatest changes can be seen in the marine-based sectors in the Ross and Weddell seas, followed by the coastal regions of West Antarctica. In East Antarctica, ice thickness increased during this period but actual constraints in East Antarctica are scarce. Compared to an ice-dynamics model such as that of Golledge *et al.* (2012), it has a greater increase in ice thickness in East Antarctica and a larger reduction in ice thickness in the Amundsen Sea sector.

IJ05_R2 (Ivins *et al.* 2013) is a revision of the IJ05 ice model (Ivins and James 2005) that is widely used to correct GRACE data. It does not include flow dynamics; instead, ice heights are adjusted to fit glacial-geological data, mostly the same as that used for W12. However, a choice was made to create the largest possible ice-thickness changes and the thickest and youngest LGM ice sheet to obtain an upper range for the GIA correction for Antarctica. In creating the ice-

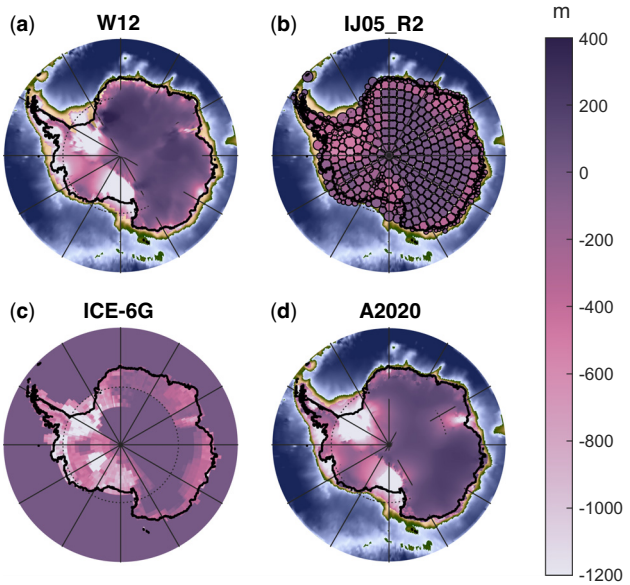

Fig. 5. Ice-thickness change between the LGM and the present for four different ice histories. LGM is taken to be 20 ka BP unless otherwise noted. Outside Antarctica, where no ice thickness existed at the LGM, the Bedmachine topography (Morlighem *et al.* 2020) is plotted. (**a**) W12 model (Whitehouse *et al.* 2012*a*). (**b**) IJ05_R2 (Ivins *et al.* 2013) with the LGM taken to be 21 ka BP. (**c**) ICE-6G_C (Argus *et al.* 2014). (**d**) A2020 (Albrecht *et al.* 2020*b*).

thickness values, the present-day ice and ocean is taken as reference: that is, only ice that is higher than the local water level corrected for the density difference, so-called ice above flotation, is outputted, as this ice thickness is the effective load in a GIA model. IJ05_R2 arrives at 7.5 m SLE that melted since 15 ka BP.

ICE-5G (version 1.2) (Peltier 2004) used limited regional constraints and ice-dome histories inferred from far-field sea-level models and records, arriving at a figure of 17.5 m SLE. This was reduced to 13.6 m SLE in ICE-6G_C (Argus *et al.* 2014). The ICE-6G_C model has been tested for consistency with an ice-dynamics simulation, by nudging the ice dynamics to the ICE-6G_C model (Stuhne and Peltier 2015). The result is a model that has a smoother shape and, for the most part, has lower ice-surface heights than ICE-6G_C. Overall, the large volume of ICE6G_C is at the high end of the range of ice-sheet reconstructions shown in Figure 3. It is also large compared to the compilation of studies in Simms *et al.* (2019), which gives an average contribution of Antarctica of 9.9 ± 1.7 m SLE, and compared to ice-sheet reconstructions that are used in GIA simulations such as W12 (Whitehouse *et al.* 2012*a*), IJ05_R2 (Ivins *et al.* 2013), and Briggs *et al.* (2014). A possible explanation is that ICE-6G_C attributes a large Antarctic contribution to the period of rapid sea-level rise known as Meltwater Pulse 1A (14.7–13.5 ka), while ice-dynamics studies Antarctic-wide generally find a smaller contribution (Mackintosh *et al.* 2011; Briggs *et al.* 2014), also supported by ice-sheet limiting data (Bentley *et al.* 2014).

A2020 (Albrecht *et al.* 2020*b*) use the Parallel Ice Sheet Model (Winkelmann *et al.* 2011) to simulate two glacial cycles. Uncertainty is quantified by varying parameters for internal ice dynamics, precipitation and mantle viscosity. The simulations are scored against present-day observations of grounded and ice-shelf areas, ice thickness, grounding-line location, and uplift rates. The model that achieved the best aggregated score shows ice thickness since the LGM to be reduced by more than 2000 m in the major shelves in West Antarctica, while ice grew by hundreds of metres in East Antarctica, similar to W12. The total volume of ice reduction is 9.7 m SLE, which is in between W12/IJ05_R2 and ICE-6G_C (Fig. 4a), and similar to other ice-dynamics-based models (Fig. 4b). A difference with the earlier discussed models is that the minimum ice volume is reached before present, with readvance and thickening occurring after 3 ka BP (e.g. at Siple Coast). Contrary to Argus *et al.* (2014), it finds that rapid Antarctica ice-sheet loss seems to be a consequence rather than a source of the meltwater pulses.

GIA model results and inferences of mantle structure

The trade-off between mantle properties and ice reconstruction is more pertinent in Antarctica, where the ice history is much less known than for other large Late Quaternary ice sheets. For a uniform viscosity and a given ice retreat, which does not vary too much spatially, GIA model simulations will show the largest uplift where the magnitude of ice change was largest: that is, at the Ross and Filchner–Ronne ice shelves, which have seen a large degree of ice retreat since 15 ka BP (Martín-Español *et al.* 2016*b*). In accordance with this relation between uplift rate and maximum ice-thickness change, the largest uplift rates are found for the ICE-6G_C (Argus *et al.* 2014) reconstruction, followed by the W12 (Whitehouse *et al.* 2012*a*) and IJ05_R2 (Ivins *et al.* 2013) ice histories (see uplift rate compilations in King 2013; Martín-Español *et al.* 2016*b*; Whitehouse *et al.* 2019). Comparison with GNSS uplift rates is not straightforward and requires correction of the GNSS uplift rates for elastic loading effects (Thomas *et al.* 2011; Scheinert *et al.* 2021, this volume), and also separation of the plate velocity and GIA models (King *et al.* 2016), as well as correcting for possible remaining tectonic effects.

GIA models based on ice models that are tuned to match GNSS or sea-level data still find an upper-mantle viscosity very close to the average global viscosity such as W12 (Whitehouse *et al.* 2012*a*), which finds a best-fit upper-mantle viscosity of *c.* 10^{21} Pa s, or IJ05_R2 (Ivins *et al.* 2013), which led to a one order of magnitude smaller best-fit viscosity (*c.* 2×10^{20} Pa s). These are the models that are applied most widely in correcting GRACE gravity measurements for the GIA signal in Antarctica (Shepherd *et al.* 2018; Scheinert *et al.* 2021, this volume).

While the GIA forward models can offer physical insight, their accuracy becomes a function of the many input parameters. Therefore, for some purposes, data-based approaches are used, which are termed 'empirical' or 'inverse' GIA models. For Antarctica, they are based on geodetic data such as GRACE time-variable gravity, satellite altimetry and GNSS (see Scheinert *et al.* 2021, this volume). Note that these are not the same as inversions of GIA models for Earth model parameters. Although the approaches are based largely on data and their error estimates, they are not entirely free from assumptions about the solid Earth such as the density of the solid Earth mass change that causes a GIA gravity change (Wahr *et al.* 2000; Riva *et al.* 2009) and an *a priori* set length-scale of GIA (Martín-Español *et al.* 2016*a*).

The forward GIA models cannot predict all of the signals seen in geodetic observations and in the empirical GIA models in West Antarctica. For instance, in a joint analysis of time-variable gravity (GRACE) data and altimetry data (Ice, Cloud, and Land Elevation Satellite (ICESat)), Groh *et al.* (2012) found a significant uplift signal of more than 20 mm a^{-1} in the Amundsen Sector in West Antarctica that is not predicted by any GIA model. The W12 (Whitehouse *et al.* 2012*a*) ice model, which accounts for ice changes in that sector during the deglaciation occurring since 20 ka BP, resulted in an uplift of at most 5 mm a^{-1} in that region. The discrepancy can be explained by the shortcomings in models that assume almost no ice-loading changes after 5 ka BP, in agreement with small change in global mean sea level during that time. However, it was later realized that the ice sheet in Antarctica responded to local climatic changes throughout the late Holocene.

A second reason for the discrepancy between data and models is that the ice in Antarctica covers a whole continent, from the East Antarctic thick crust to the West Antarctic thinner one, which cannot be truly represented by a single viscosity profile. As stated earlier, substantial differences exist in the Earth's structure between East and West Antarctica: warmer and weak mantle beneath West Antarctica and colder and stiffer mantle beneath the East Antarctic Craton (Berg *et al.* 1989; Morelli and Danesi 2004; Hansen *et al.* 2014; Martin *et al.* 2014; An *et al.* 2015; Burton-Johnson *et al.* 2020; Wiens *et al.* 2021, this volume). East Antarctica shows high seismic velocities down to a depth of 200 km, correlating with old structures, although velocities at the coast are close to the global average of around 150 km and deeper. The Ross and Weddell seas have modest positive anomalies, and the slowest velocities are found in the part of West Antarctica where Cenozoic rifting and extension took place, particularly in Marie Byrd Land, the Amundsen Sea sector and the Antarctic Peninsula. The slow velocities do not extend very deep beneath the Antarctic Peninsula, where fast anomalies are found in the transition zone, but for Marie Byrd Land they do extend deeper. Seismic velocity can be used to calculate viscosity anomalies but with several assumptions and with uncertainty resulting from unknown conversion factors and the varying quality of the seismic model. Therefore, other

sources of information are necessary to infer mantle structure, as reviewed in this volume. For Antarctica, these can include gravity and magnetic data (Pappa and Ebbing 2021, this volume), geology (Panter and Martin 2021, this volume) or mantle xenoliths (Handler *et al.* 2021, this volume; Martin 2021, this volume).

The high mantle viscosity used in traditional GIA models makes the predicted effect of ice changes within the last few hundred years negligible. In several regions on Earth, adjustment is much faster; the response to the LGM load has all but relaxed and the current uplift is caused by deglaciation events in the last few centuries. This is the case for glaciated regions near ridges such as Iceland (e.g. Sigmundsson 1991), and near subduction zones such as Alaska (e.g. Larsen *et al.* 2005) and Patagonia (e.g. Dietrich *et al.* 2010), where mantle conditions clearly deviate from the global average. For these areas, local modelling is required combined with a local deglaciation history for the last few centuries. The possibility of a large signal due to local, recent ice unloading in Antarctica was hinted at in Ivins *et al.* (2000). In the last decade, the availability of GNSS data has enabled the development of regional GIA models that include changes in ice thickness over the last few centuries. Regional studies can provide a constraint on regional upper-mantle viscosities that together can lay out a picture of a varying mantle structure, which can be compared to other observations of the Earth's structure,

The best-fitting upper-mantle viscosity from regional GIA studies that can be compared to the geophysical image of Antarctica's mantle are discussed in the following. To match the observed uplift rate data, the regional studies need to include elastic deformation due to current ice-thickness changes and the response to recent ice-loading changes in a period that is sometimes called the Little Ice Age, although confusingly this period is not the same for different regions on Earth. Nield *et al.* (2014) analysed GPS uplift histories in the northern Antarctic Peninsula and found that geodetic uplift rates greatly exceeded their estimates for the Earth's purely elastic response to contemporary ice-mass changes, implying a significant viscous component of uplift. They concluded that the observed uplift rates after subtracting elastic deformation could be explained by invoking upper-mantle viscosities in the range 0.6×10^{18}–2×10^{18} Pa s. A similar range of 0.3×10^{18}–3×10^{18} Pa s was found in a more recent analysis by Samrat *et al.* (2020). Best-fit upper-mantle viscosity ranges are presented as coloured ellipses encompassing the respective study regions in Figure 6 on top of 3D viscosity maps from Ivins *et al.* (2021, this volume) at two depths in the upper mantle. Note that the tip of the Antarctic Peninsula does not have the lowest viscosity based on the 3D viscosity maps, especially at a depth of 300 km, which indicates the uncertainty in translating seismic velocities to viscosity.

The best-fit viscosities obtained can also be compared to the tectonic setting of the northern Antarctic Peninsula. Along the western Peninsula, a subduction zone, which shut down progressively from south to north between 50 and 4 Ma (Barker 1982; Larter and Barker 1991; Eagles *et al.* 2004), remains active along the South Shetland Trench and has an active back-arc basin (Lawver *et al.* 1996). The Bransfield Straight, separating the South Shetland Islands from the northern tip of the peninsula, is undergoing extension and there is evidence of active volcanism (Barker and Austin 1998; Smellie 2021). This means that a viscosity below the global average is not unexpected there. The low viscosities were confirmed by Samrat *et al.* (2021) in the northern Marguerite Bay, with viscosities found to range from 0.1×10^{18} to 9×10^{18} Pa s. This matches the slow seismic wave speeds along the Western Antarctic Peninsula (see the background viscosity map and Wiens *et al.* 2021, this volume). In the southern part of the Antarctic Peninsula, viscosity appears to be higher (Zhao *et al.* 2017), in agreement with past subduction that ended from south to north. Uplift rates due to the thinning of the Wordie Ice Shelf match the small GPS uplift rates observed there only for a lower bound of viscosity of 2×10^{19} Pa s. This larger viscosity implies that viscosity increases by an order of magnitude over 500 km.

Other examples include studies in the Weddell Sea, where the uplift rate allows tentative conclusions on the timing of retreat. Wolstencroft *et al.* (2015) argued for a later retreat than assumed in the Antarctic-wide ice reconstructions (Whitehouse *et al.* 2012*a*; Ivins *et al.* 2013; Argus *et al.* 2014), and Bradley *et al.* (2015) argued for retreat from the 6 ka grounding line and subsequent readvance. Wolstencroft *et al.* (2015) found best agreement with an upper-mantle viscosity somewhat larger than in the rest of the Antarctic Peninsula, although the evidence is not very conclusive. In East Antarctica, few data are available; a recent study by Hattori *et al.* (2021) showed uplift rates in Lützow-Holm Bay, East Antarctica, that agree with some of the global GIA models.

Barletta *et al.* (2018) analysed geodetically observed uplift rates in the Amundsen Sea Embayment, West Antarctica, by

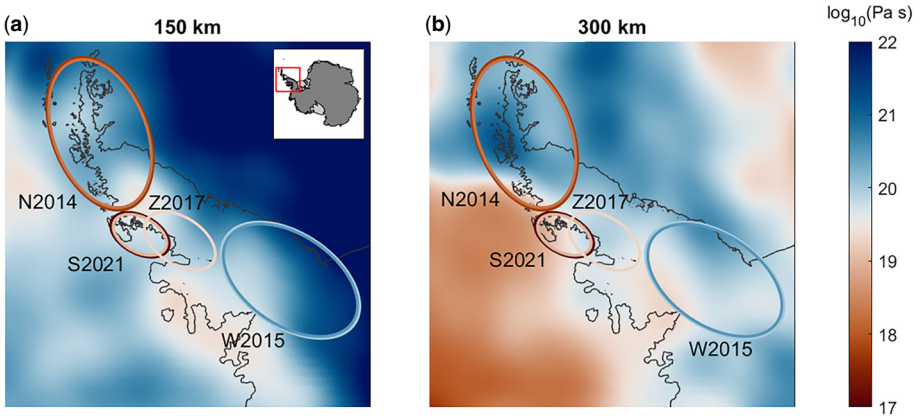

Fig. 6. 1D upper-mantle viscosity constraints $\log_{10}$(Pa s) from GIA studies in the Antarctic Peninsula. The location of the ellipse outlines roughly the region for which the viscosity constraint is obtained; the colour denotes the viscosity; the outer ellipse is the lower bound of the best-fit viscosity range and the inner ellipse is the upper bound. N2014, Nield *et al.* (2014); Z2017, Zhao *et al.* (2017), who only provide a minimum viscosity; W2015, Wolstencroft *et al.* (2015); S2021 (Samrat *et al.* 2021). (**a**) The background is the 3D viscosity map from Approach 3 in Ivins *et al.* (2021, this volume): i.e. derived from the Antarctic seismic model of Lloyd *et al.* (2020) for dry olivine with a 4 mm grain size and stress of 0.1 MPa at 150 km depth (**a**) and at 300 km depth (**b**).

modelling the horizontal and vertical displacement of all Antarctic GPS Network (ANET) stations in the Amundsen sector. The rate of ice-mass loss there is the major part of the ice-mass loss of the entire Antarctic Ice Sheet. Ice loss since 1890 in combination with satellite-observed ice loss and a shallow upper-mantle viscosity of 4×10^{18} Pa s gave best fit to the GPS uplift rates. Despite the fact that this region is far removed from any plate boundary, it is underlain by slow seismic velocities. There are also indications of geologically recent (and, perhaps, locally active) rifting in much of West Antarctica, including the Amundsen sector (Wobbe *et al.* 2012). An example are the indications of active volcanism (Smellie *et al.* 2021), and Cenozoic rifting in much of West Antarctica, and limited evidence that points to rift-related displacements of Oligocene age between the Thurston Island–Eights Coast and Marie Byrd Land crustal blocks flanking the Amundsen sector (Kalberg *et al.* 2015; Spiegel *et al.* 2016). This supports the finding of Barletta *et al.* (2018) that mantle viscosity in this region deviates significantly from the global average.

The regional studies are well suited to fit uplift rates but they fall short in representing the continental-scale signal seen by the GRACE mission as there is a contribution from the far-away ice sheets through the global sea-level variations and associated continental levering. In terms of mass change, this contribution is almost 40% of the post-LGM signal (Caron and Ivins 2020). Moreover, regional GIA models in Antarctica do not simulate the effect of neighbouring regions with a different viscosity, which is represented in Figure 1 as deformation in the mantle that is not symmetrical with respect to a vertical cross through the centre of the ice sheet. Thus, 3D GIA models should probably be used for some parts of Antarctica despite their longer computation time. A possible faster solution is the combination of multiple regional 1D solutions, as in Hartmann *et al.* (2020), or an ELRA model with regional parameters (Coulon *et al.* 2021) but their accuracy should be further investigated.

3D GIA studies require viscosity maps as input, which can be derived from seismic velocity anomalies, as reviewed in Ivins *et al.* (2021, this volume). Therefore, an anomaly in seismic velocities can be converted to an anomaly in temperature, which can be related to anomalies in logarithmic viscosity using scaling factors based on laboratory measurements. GIA studies using 3D models have mostly followed this approach, with more recent models taking advantage of more seismic data and full-waveform inversion that yield more accurate velocity estimates. Ivins *et al.* (2021, this volume) discuss and quantify some of the uncertainties: the scaling factors, the background temperature profile and other parameters in the creep laws of mantle rocks, resulting in a standard deviation of 1 in logarithmic viscosity, mainly in areas with high viscosity. This is not yet the full uncertainty range: seismic velocity anomalies have uncertainties that are hard to quantify. Furthermore, water content can affect seismic velocities directly and can also affect deformation for a given temperature. Water content varies within the Antarctic mantle (Martin 2021, this volume).

Thus, results of 3D models should be assessed with this uncertainty in mind. However, it should also be realized that because of the way that 3D viscosity maps for GIA studies are created, the 3D GIA models do not have many more degrees of freedom in fitting GIA observations than 1D GIA models. Mostly, it is assumed that viscosity can be obtained by scaling seismic velocity perturbations (Kaufmann *et al.* 2005; Geruo *et al.* 2013; Hay *et al.* 2017; Powell *et al.* 2020), as discussed by Ivins *et al.* (2021, this volume). There are a number of choices for parameters that change the amplitude of this spatial pattern, in addition to assumed background temperature or background viscosity, but the spatial pattern is determined by the seismic model used. A somewhat different approach translates the velocity anomalies into temperature anomalies, which are entered into a mantle flow law (van der Wal *et al.* 2015; King *et al.* 2016; O'Donnell *et al.* 2017). In this case, viscosity can also depend on the stress in the mantle, as will be discussed later. Even so, the spatial pattern in effective viscosity will be determined mostly by the pattern of the seismic velocity anomalies. This means that a better fit of 3D models compared to 1D models should not be expected automatically when using spatially homogeneous scaling parameters. 3D GIA models by themselves allow variations in viscosity for each element in the model, and some applications in the future might require fitting spatial variations in parameters directly, in which case the number of degrees of freedom will be much greater and inversions become more problematic. In this case, other information such as gravity anomalies (Pappa and Ebbing 2021, this volume) and geologically derived constraints can also be helpful (Burton-Johnson *et al.* 2020; Martin 2021, this volume; Martin *et al.* 2022, this volume).

An approach that can be followed to reduce uncertainty in 3D viscosity maps is to calibrate the 3D viscosity estimates with regional 1D studies. Viscosity values that can serve as such anchor points are compiled in table 6 of Ivins *et al.* (2021, this volume) and in figure 1 of Lau *et al.* (2021). Ivins *et al.* (2021, this volume) conclude that rheology derived from micromechanics and seismology compares well with viscosities derived from GIA models for several regions. In particular, the low viscosity in the Antarctic Peninsula can be replicated. A selection of studies for the Antarctic Peninsula is shown in Figure 6 together with a 3D viscosity estimate from Ivins *et al.* (2021, this volume). An important caveat is that it is not immediately clear if the best-fit 1D viscosity should be seen as an average over a certain part of the mantle. The question becomes: To what region and depth is a certain observable sensitive? We know from the sensitivity kernels discussed earlier that larger ice sheets are sensitive to deeper structure. However, the sensitivity itself depends on the viscosity profile. Sensitivity is concentrated in areas of low viscosity in the case of a viscosity contrast. In that case, the low viscosities have a larger weight in determining what 1D viscosity corresponds best to the 3D viscosity pattern. It could be advocated that a viscosity representative of the process should be weighted by strain rate or by internal work (Christensen 1984). Blank *et al.* (2021) used the approach of averaging only over those elements where the stress reaches a threshold value, relative to the maximum stress.

In 1D models, the lithospheric thickness is an independent input parameter. It is difficult to quantify lithosphere thickness based on other studies because the lithosphere is defined differently in different fields. For GIA, a suitable definition is the top part of the Earth that deforms elastically on the timescale of the glacial loading considered (e.g. Nield *et al.* 2018). This is different to a definition of lithosphere based on seismic wave speed (e.g. Wiens *et al.* 2021, this volume), from the elastic layer that is considered in gravity data (e.g. Pappa and Ebbing 2021, this volume) or the chemical-compositional-melt boundary considered from mantle xenolith data (Coltorti *et al.* 2021, this volume), see also Rychert *et al.* (2020). A further consequence of the GIA definition of effective lithosphere is that its thickness changes in time; for the same 3D Earth structure, the effective lithosphere for will be thicker when studying a response on the timescale of centuries than for a timescale of thousands of years. An advantage of using 3D viscosity is that it is no longer necessary to prescribe the lithosphere thickness *a priori*.

The influence of lateral viscosity on observables in Antarctica can be determined by comparing the outcome of 3D and 1D GIA models. The effect on uplift rate was found to be

around 1–2 mm a^{-1} (Kaufmann *et al.* 2005; Geruo *et al.* 2013), which is relatively small, especially considering the larger ice sheets used in these studies compared to latest Antarctic Ice Sheet reconstructions. A change in the location of the maximum uplift rates can also be observed (e.g. comparing fig. 5b and c of Kaufmann *et al.* 2005 to their fig. 4b and c; van der Wal *et al.* 2015). This can be explained by the different time sensitivities: a higher viscosity will be sensitive to earlier ice-load changes that could have occurred at a different location. For the mass balance of the Antarctic Ice Sheet observed by the GRACE mission, van der Wal *et al.* (2015) found an effect of 3D viscosity of up to 20 Gt a^{-1} compared to current ice-mass loss of 160 Gt a^{-1}. Blank *et al.* (2021) showed that lateral changes in viscosity cannot as yet be detected in GPS measurements in the Amundsen Sea sector. Focusing on the spatial pattern of uplift rates, Nield *et al.* (2018) observed that the 3D models result in a higher amplitude and shorter wavelength, which is due to the thinner effective lithosphere that can warp easier.

For horizontal velocities, the effect of 3D viscosity variations is larger than for vertical uplift rates, as found by sensitivity studies (Wu 2006). The effect of viscosity variations is such that the horizontal displacement rate can be reversed depending on viscosity, as the horizontal rates are a resultant of two opposite motions: the lithosphere that flexes such that points move away from the former ice sheet, while the underlying mantle flows towards the ice-covered region (Hermans *et al.* 2018). For Antarctica, the stiff cratonic root of East Antarctica is thought to promote flow in the weaker West Antarctic mantle (Kaufmann *et al.* 2005), which might be visible in horizontal GNSS observations there (Konfal *et al.* 2018). An enhanced effect of 3D viscosity on horizontal velocities is also found for uplift caused by ongoing ice melt in West Antarctica (Powell *et al.* 2020).

Finally, in terms of RSL data, Gomez *et al.* (2018) found an effect of 3D rheology of tens of metres across Antarctica, well above the measurement accuracy. The sensitivity of RSL data depends greatly on the ice history. Bagge *et al.* (2021) found a large sensitivity to lateral variations in the Ross Sea, and they explain this by the relatively thin ice sheet compared to the ice sheets in classical GIA areas, which makes the response more sensitive to shallower layers where larger lateral variations exist.

Apart from lateral variations, the predictions in Antarctica are also sensitive to the presence of a power-law rheology, which results in stress-dependent rheology (Nield *et al.* 2018; Blank *et al.* 2021). Such a power-law rheology represents behaviour that is observed in deformation experiments: steady-state creep proceeds faster when stress is higher. This implies that effective viscosity depends on stress and changes in time: effective viscosity is lower where and when stress is high. This local weakening leads to larger peaks in uplift rate (Nield *et al.* 2018; Blank *et al.* 2021). During the glacial cycle, the change in viscosity can be up to two orders of magnitude (Barnhoorn *et al.* 2011). That has an important implication, namely that the viscosity that is valid for the glacial cycle is not necessarily the same viscosity that holds for a more recent loading process, or a longer term process such as mantle convection (Bredow *et al.* 2022, this volume). Figure 7 shows the change in viscosity in the Amundsen Sea sector as a result of stress from post-LGM ice loss for two different 3D viscosity models. The model in the top row has lower temperatures but, because the grain size is smaller, viscosity is on average lower than the bottom model (further details are given in Blank *et al.* 2021). The change in viscosity as a result of the post-LGM decline of the West Antarctic Ice Sheet ranges by up to two orders of magnitude for the model with a stiff rheology (top row) and a long 'memory' (Fig. 7), although the change is greatest for shallow regions where viscosity is so high that it can be considered to be part of the lithosphere.

Note that the stress-dependent rheology is not the same as transient rheology. Experiments show anelastic or transient rheology before steady-state creep is reached (Faul and Jackson 2015). In its simplest form, transient rheology can be parametrized by a short-term and long-term viscosity (e.g. Caron *et al.* 2017). Such a rheology is used more often in post-seismic deformation studies and will be discussed in the following 'Post-seismic deformation' section. The description of transient rheology can be more general than short-term v. long-term viscosity; experiments show that the rheology, in general, depends on the frequency of loading (Ivins *et al.* 2020). Accounting for this frequency dependence, Lau *et al.* (2021) calculated a complex viscosity for Antarctic regions for a mantle composition based on olivine and with a dependence on grain size. At a frequency between long-term and short-term GIA, the transient process is shown to make a large contribution (Lau *et al.* 2021). This also leads to an effective viscosity that changes in time, which is conceptually different from a stress-dependent rheology.

Coupling of ice to solid Earth: feedbacks and processes

As noted in the introduction to this chapter, the deformation of the solid Earth affects the dynamics and growth of the ice sheet on top of it. Thus, solid Earth deformation is important for the

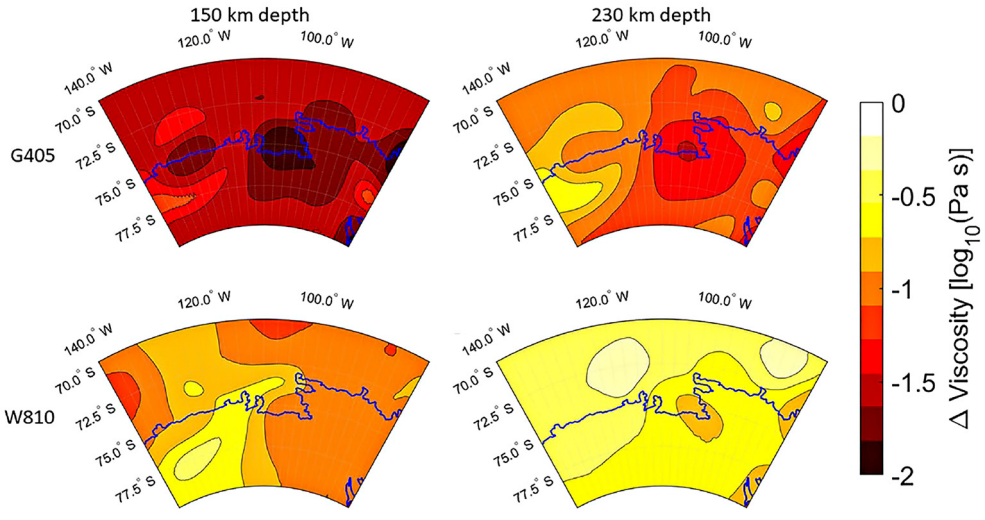

Fig. 7. The change in viscosity as a result of stress from the last glacial cycle at the start of the simulation for the Amundsen Sea Embayment in AD 1900. G405 is a 3D viscosity model based on a gravity-derived lithosphere model for Antarctica (Pappa *et al.* 2019) using an olivine flow law with a grain size of 4 mm and water content of 500 ppm. W810 is based on a global temperature model (an early realization of WINTERC-G of Fullea *et al.* 2021) using an olivine flow law with a grain size of 8 mm and 1000 ppm water content. Source: adapted from Blank *et al.* (2021).

ice sheet in the last glacial cycle but also for scenarios of future Antarctic Ice Sheet decline. In this subsection, the main effects are discussed, how they are modelled and what the implications are of variations in mantle viscosity.

GIA influences ice dynamics in different ways. A straightforward effect is that it brings the ice surface to a different altitude (schematized in Fig. 1) and hence to a different atmospheric temperature that might promote or inhibit melting. However, in Antarctica, temperatures are low everywhere and the greatest influence of the evolving topography induced by GIA is on the grounding-line position of the ice sheet. The grounding line lies at the transition between grounded ice and floating ice. Its position is influenced by the local ice thickness and the local sea level. A rise in sea level is associated with a grounding line that moves inwards (Hollin 1962). As the ice sheet gets thinner, the grounding line retreats inland and the amount of floating ice increases. Ice discharge scales with ice thickness at the grounding line. Therefore, if the depth of the bedrock increases inland, the ice-thinning rate increases more, a phenomenon termed 'marine ice-sheet instability' (Weertman 1974; Schoof 2007). As a result of a decreased ice load, the bedrock beneath the ice sheet uplifts, which causes the grounding line to shift back towards the ocean, leading to a decrease in melt and a reduction in discharge if topography reduces outwards. The main effect of GIA is therefore a negative feedback that stabilizes the Antarctic Ice Sheet, specifically at regions where the bedrock uplift is fast (e.g. Parizek and Alley 2004; Kachuck *et al.* 2020). When this coupling is considered, the palaeo-ice volume is 1–2 m SLE smaller (Whitehouse 2018). The uplift is also called upon to explain a readvancing grounding line in the late Holocene (e.g. Kingslake *et al.* 2018) and as a slowing effect on the Amundsen Sea sector ice-sheet retreat (Johnson *et al.* 2020).

A second effect related to GIA that modulates the ice dynamics is the sea-level fall due to a decrease in the gravitational attraction of a melting ice sheet. The sea-level fall will lead to an outward-moving grounding line and a decreased flux across the grounding line, once again promoting a negative feedback (Gomez *et al.* 2010). However, sea level can also change in response to other ice sheets or processes. The sea-level forcing due to northern hemisphere ice sheets was shown to increase the amount of ice loss since the LGM, and hence the size of the LGM ice sheet (Gomez *et al.* 2020). Furthermore, smaller feedback effects of GIA in Antarctica are an altered bed slope that could stabilize the ice sheet even more and the rise of pinning points at ice shelves as a result of bedrock uplift (Adhikari *et al.* 2014; Whitehouse *et al.* 2019). Pinning points, which can arise due to natural topography roughness (e.g. tectonic or volcanic features) or can be built by the ice sheet itself (Colleoni *et al.* 2022), can act as 'brakes' on the flow of the glacier. In reality, all feedback effects work together. For example, in the Weddell Sea, ice regrounded in the late Holocene is likely to have occurred due to the rebound of a topographical feature that formed an ice rise (Siegert *et al.* 2019). This was helped by the lowering of the water depth and smaller self-attraction.

To compute the solid Earth deformation, ice-dynamics models generally employ a fast approximation of GIA using an ELRA model to simulate GIA (e.g. Golledge *et al.* 2014; Maris *et al.* 2014; Pollard *et al.* 2016). In this model, it is assumed that the Earth, consisting of two flat layers, responds to a certain change in ice load by deforming exponentially towards the equilibrium displacement for that particular ice height (Le Meur and Huybrechts 1996). The time needed to reach equilibrium, the relaxation time, is typically taken to be 3 kyr for the Antarctic continent, which resulted in a present-day topography that was in agreement with that computed with a more realistic GIA model (Le Meur and Huybrechts 1996). More realistic GIA models include the physics of a layered Earth that differs from the ELRA model in several aspects. Even for a two-layered Earth, the relaxation-time response depends on wavelength, while for the ELRA model it does not. In addition, the forebulge is more pronounced in a GIA model and GIA models allow the inclusion of more layers. The difference in the LGM ice volume between coupling with an ELRA or GIA model can be more than 2 m SLE (Whitehouse *et al.* 2019). An intermediate case in between the ELRA and GIA models is the viscoelastic half-space, where relaxation time depends on the size of the ice sheet (e.g. Bueler *et al.* 2007; Garbe *et al.* 2020). This has been used by Albrecht *et al.* (2020*a*) to show that low mantle viscosity fits better to the observed ice flow, while higher viscosity fits better to GPS uplift-rate data.

Several ice-sheet models have been developed that are coupled to 1D GIA models: for example, GIA models based on the normal-mode method (e.g. Gomez *et al.* 2012; de Boer *et al.* 2014) or the spectral finite-element method (Konrad *et al.* 2014, 2015). Important parameters in the coupling are the spatial resolution of the ice-sheet model with which the model represents the bedrock and grounding line, and the time resolution, especially in areas with low viscosity and fast response. The ice-sheet model requires an initial topography, for which present-day topography is used, corrected with the deformation caused by GIA over the glacial cycle (Gomez *et al.* 2013). An example of the topographical deformation for a 3D GIA model based on the W12 ice-loading history (Whitehouse *et al.* 2012*a*, b) and olivine rheology (4 mm grain size as in Ivins *et al.* 2021, this volume, Approach 3) resulted in maximum displacements of 130 m for the Weddell Sea and 117 m for the Ross Sea.

To include the effects of GIA on sea level through the change in gravity, GIA feedback has also been modelled using coupled ice dynamics–sea level models (Gomez *et al.* 2013; de Boer *et al.* 2014; Konrad *et al.* 2015; Pollard *et al.* 2017; Larour *et al.* 2019). Here the sea-level model computes both the bedrock deformation and the RSL change following a change in the equipotential surface, and forwards this to the ice-sheet model. Although coupled ice sheet–sea level models are computationally more expensive than the ELRA model, a varying temporal resolution can be used to decrease computation time by 50% (Han *et al.* 2022). A disadvantage of such an algorithm is that, with the usual sea-level algorithm for every time step, the entire ice history needs to be convolved with the Earth's response.

Ice-sheet models have also been coupled to 1D GIA models that are more consistent with seismological and geological evidence of the structure under the Antarctic Ice Sheet (Gomez *et al.* 2015). Less ice loss is predicted when using a structure consistent with the rheology under the West Antarctic Ice Sheet compared to using a structure derived from globally distributed ice-age datasets. DeConto *et al.* (2021) showed the limited effects of a relatively low mantle viscosity on Antarctic ice retreat in the coming two centuries using a coupled ice sheet–1D GIA model. However, tailoring the model for a certain region cannot always replace a model with true lateral variations, given the large region to which the ice sheet is sensitive and the large variations in viscosity across the Transantarctic Mountains and within the Antarctic Peninsula. Predictions of sea-level fall as a result of a West Antarctic melt event increase by 20 and 50% in the coming decades compared to purely elastic deformation when using a 1D and 3D rheology, respectively (Hay *et al.* 2017). It should be noted that the 1D viscosity in this study was relatively high (10^{21} Pa s), which subdues the response of the 1D model. On the other hand, due to the uncertainties in the conversion from seismic velocity to viscosity anomalies, the prediction of sea-level fall can be even larger for different 3D models. This shows the importance of the tuning of the

model to the local Earth properties, both for 1D and 3D models. To know whether a 3D model is really necessary or if 1D models are sufficient, locally tuned 1D models should be used, as for example, in Blank *et al.* (2021).

Full 3D GIA models have large computation times of the order of days to weeks. Therefore, shortcuts have been proposed: the ELRA model with laterally varying relaxation time (Oude Egbrink 2017) or laterally varying flexural rigidity, or both (Coulon *et al.* 2021). While these can simulate the differences in relaxation time that exists, for example, between West and East Antarctica, they cannot capture the full physics of stress transfer from a region of higher to lower viscosity or vice versa. To study the effect of lateral variations on the evolution of the Antarctic Ice Sheet, Gomez *et al.* (2018) coupled an ice sheet model to a 3D GIA model for the past 40 kyr by iterating the initial topography until the present-day topography was achieved. Significant differences in ice loading were found; the grounding line retreated less during the deglaciation phase when using a 3D rheology tuned for Antarctica compared to using a 1D rheology not tuned for (part of) Antarctica. During the deglaciation phase, ice thickness was up to 1 km thicker in the Ross Sea when using 3D GIA, although still far from the present-day ice sheet. The enhanced flexibility of 3D model makes it suitable for those complex regions but its uncertainty is large without validation against data such as RSL or present-day ice cover.

The coupling is also relevant at other timescales, such as the Eocene–Oligocene transition (34–33.5 Ma BP), the Last Interglacial (130–116 ka) and future Antarctic ice loss. These will be discussed briefly in the following. In the Eocene–Oligocene transition, the Antarctic Ice Sheet emerged or became more prominent (Miller *et al.* 1991; Lear *et al.* 2000). At that time, the same physics applies as in the Pleistocene ice sheet; a growing ice sheet attracts and raises sea level. The resulting GIA effects modulate the ice sheets as the forebulge progresses through the edges of the Antarctic continental shelf (Stocchi *et al.* 2013). Sea level at this epoch, recorded in drill cores, reflects the competing effects of attracting sea level from the growing ice sheet, and the forebulge from the growing East Antarctic Ice Sheet (Galeotti *et al.* 2016). For Pliocene studies, the role of GIA is that of correcting sea-level measurements, as well as providing corrections on the initial topography on which the ice sheet formed (e.g. Rovere *et al.* 2014). As these studies can be probably considered preliminary from a GIA modelling point of view, there is room for improvement by including recent insights into the mantle structure of Antarctica.

The last interglacial saw smaller ice sheets on Antarctica, which provides a pessimistic window on the stability of the Antarctic Ice Sheet in a warming climate. Estimates for sea level at the last interglacial show a much higher sea level, of which 3–4 m SLE might have come from extra melting of the West Antarctic Ice Sheet beyond its present configuration (e.g. Turney *et al.* 2020). The sea-level change is partly controlled by GIA, with several decimetres found to have been determined by lateral variations in viscosity as a result of meltwater expulsion from rapid bedrock uplift due to low viscosity in West Antarctica (Pan *et al.* 2021; Powell *et al.* 2021).

The low viscosity will also act to slow the future decline of the West Antarctic Ice Sheet. Although earlier simulations concluded that the effect of bedrock uplift was minor (Bamber *et al.* 2009; Mitrovica *et al.* 2009), it is enhanced for low viscosity (Konrad *et al.* 2015; Barletta *et al.* 2018). For West Antarctic Ice Sheet collapse, the deformation of a 3D model reaches more than 50% of the elastic deformation after 100 years (Hay *et al.* 2017). Larour *et al.* (2019) found that uplift has a small effect (*c.* 1% in 2100), increasing to 27% after 500 years, which makes it a relevant process to take into account in future scenarios for the Antarctic Ice Sheet. To do so, spatial resolution is important, in particular near the grounding line where the coupling manifests. A resolution of 1 km is suggested for elastic effects (Larour *et al.* 2019) and a value of about 4 km is suggested for modelling the viscous effects (Wan *et al.* 2022). These resolutions can be reached by 3D GIA models but with increased computation time compared to standard GIA simulations. When many scenarios should be simulated, regional (flat) GIA models or ELRA models with spatially varying parameters can be a pragmatic choice but it is not yet clear how much they deviate from full 3D spherical GIA models.

Post-seismic deformation

Earthquakes are the result of the sudden release of built-up strain on a fault plane within the Earth's lithosphere. Most earthquakes occur at tectonic plate boundaries and are associated with the relative motion of the plates as they slowly move past each other (transform plate boundary), collide (convergent plate boundary) or separate (divergent plate boundary). Part of the interface at the plate boundary may become locked due to frictional resistance, preventing the two plates from moving past each other and resulting in an accumulation of strain. At a critical point in time, the accumulated strain becomes larger than the frictional resistance, the fault unlocks and the plate interface suddenly moves, causing an earthquake and a change in stress in the surrounding crust and mantle.

A small number of earthquakes also occur in the interior of a tectonic plate, termed 'intraplate earthquakes', although these earthquakes are not as common as those occurring at plate boundaries. The cause of intraplate earthquakes is not well understood but it has been suggested that they may occur due to pre-existing structures or weaknesses within the tectonic plate (Stein and Mazzotti 2007).

Earthquakes cause deformation at the Earth's surface from several processes (see Fig. 8) that can be categorized as coseismic or post-seismic, depending on whether they occur at the time of, or following, the earthquake. Coseismic displacement is the instantaneous slip that occurs on the fault plane at the time of the earthquake and the associated elastic response of the Earth in the surrounding region. Following this initial coseismic displacement, the Earth undergoes subsequent post-

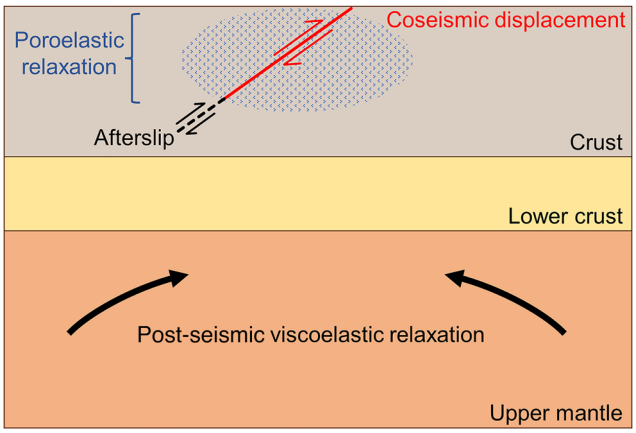

Fig. 8. Schematic representation of earthquake deformation processes. Fault-plane and coseismic displacement is shown in red, with deep afterslip shown as a black dashed line. The blue shaded region indicates poroelastic relaxation and black arrows in the upper-mantle show where post-seismic relaxation may occur.

seismic deformation caused by several processes (Wright 2016). Afterslip, which is the subsequent slow slip on the fault plane controlled by friction, usually occurs above or below the location of seismic rupture (e.g. Fig. 8). Changes in fluid pressure in the shallow upper crust close to the fault (e.g. Fig. 8) can cause poroelastic relaxation to occur in the months following an earthquake. Poroelastic relaxation takes into account the stress change due to movement of a fluid through a porous solid matrix. Finally, viscoelastic relaxation within the lower crust and upper mantle occurs as the viscous material responds to stress changes. Because this second process occurs at depth, it produces a longer wavelength signal and, hence, is the dominant cause of surface deformation in the far field (typically more than 300 km from the earthquake). Post-seismic viscoelastic deformation from large earthquakes (greater than magnitude 9) can be observed over 1000 km away from the epicentre (Shao *et al.* 2016) and can be sustained over several decades. For example, deformation from the 1960 Chile earthquake, with a magnitude of 9.5, was still being observed *c.* 40 years after the event (Khazaradze and Klotz 2003).

In this section, we will focus on post-seismic viscoelastic deformation, explore what it might reveal about the underlying mantle and outline some results for Antarctica where the study of post-seismic deformation is still in its infancy.

Post-seismic deformation, observations and models

The sudden large stress change associated with an earthquake causes viscoelastic relaxation of the lower crust and upper mantle over the years and decades following an earthquake. The magnitude, spatial pattern and time evolution of the deformation is dependent on the size of the earthquake, the geometry of the fault plane and the rheological properties of the Earth.

Post-seismic viscoelastic deformation can be observed by increasingly dense networks of geodetic measurements such as GPS (e.g. Freed *et al.* 2012) and InSAR (Interferometric Synthetic Aperture Radar: e.g. Wang and Fialko 2018), motivating the development of models to help to interpret geodetically observed deformation (see also Scheinert *et al.* 2021, this volume) and to fill in the gaps between observations in space and time. Through a process of varying model inputs and comparing model predictions to observations, constraints can be placed on the likely Earth structure (Pollitz 2005) or rheological model (Freed *et al.* 2012). In particular, the viscosity of the mantle has a dominant control over the response of the Earth to an earthquake.

Modelling techniques used for post-seismic deformation include the normal-mode method that is also widely applied in GIA modelling. The widely used VISCO1D program of Pollitz (1997) has been used in Antarctica (King and Santamaría-Gómez 2016) but it can only deal with radially varying parameters that might not be appropriate for a large part of Antarctica. Finite-element methods exist with half-space geometry (e.g. Freed *et al.* 2012) or with spherical geometry (Hu and Wang 2012; Agata *et al.* 2019). The latter are not global and do not include self-gravity, as the normal-mode method does, which can be relevant for large earthquakes. Recently, a global spherical finite-element method was presented that does include self-gravity (Nield *et al.* 2022), and has capabilities to include different rheological models and the sea-level equation, which is relevant for earthquakes under the ocean (e.g. Broerse *et al.* 2011).

Estimating post-seismic viscoelastic deformation via modelling techniques requires detailed knowledge of the earthquake such as location, depth, fault geometry and slip parameters. This information can often be found from studies of fault inversions, whereby slip properties are deduced through the inversion of the seismic observations (e.g. Ji *et al.* 2002; Hayes 2017) or from geodetic inversions (e.g. Lohman and Simons 2005; Feng *et al.* 2010). The properties of the Earth (e.g. mantle viscosity and elastic properties) and rheological model (e.g. Maxwell or Burger rheology: see Ivins *et al.* 2021, this volume), which are used as input to a forward model of post-seismic viscoelastic deformation, are then varied and the predicted displacements tested against geodetic observations, similar to GIA studies (see the 'GIA model results and inferences of mantle structure' subsection in the previous section). Alternatively, the Earth properties can be inverted using gradient-based optimization with the required gradients computed efficiently using the adjoint method (Crawford *et al.* 2017).

The rheological model can be of particular importance in the study of post-seismic deformation. The short timescale of stress change involved means that transient effects, where the short-term mantle viscosity is lower than the long-term steady-state viscosity, are important (Ranalli 1995). Several studies have shown that a transient component of deformation in addition to a steady-state viscosity is required to explain observations, specifically Burger's rheology (Pollitz and Thatcher 2010) or transient power-law rheology (Freed *et al.* 2010, 2012). This is in contrast to GIA, where non-linear or transient rheologies have been used but do not always improve the fit (van der Wal *et al.* 2015; Caron *et al.* 2017).

Insights from other regions

The study of post-seismic deformation in Antarctica is still in its infancy; however, there are many studies that have successfully constrained mantle properties or rheology in other regions of the world. The 1960 magnitude 9.5 earthquake in Chile was the largest earthquake to have ever been recorded. It occurred at the convergent plate boundary where the Nazca Plate is subducting below the South American Plate. The earthquake occurred long before the geodetic measurements of the Chile subduction zone commenced in 1993; however, the signature of the post-seismic deformation is still visible in observations 35 years after the earthquake (Hu *et al.* 2004). Several studies have constrained the continental upper-mantle viscosity in this region to 2×10^{19}–3×10^{19} Pa s using a 3D linear Maxwell viscoelastic model (Khazaradze *et al.* 2002; Hu *et al.* 2004). Sun *et al.* (2018) also explored the possibility of a Burger's rheology for the 1960 event; however, due to the length of time between the earthquake and the beginning of the GPS measurements, it was not possible for them to constrain a value for the transient viscosity. Their results for the steady-state viscosity of the mantle wedge above the subducting slab (2×10^{19} Pa s), constrained with GPS observations, agree with studies mentioned above.

In Alaska, a magnitude 7.9 strike-slip earthquake occurred on 3 November 2002. GPS stations recorded deformation rates of up to 300 mm a^{-1} during the month following the earthquake and up to 100 mm a^{-1} during the subsequent 18 months (Pollitz 2005). Pollitz (2005) interpreted the two distinct deformation rates as being indicative of a Burger's rheology with an initial transient viscosity and a long-term steady-state viscosity. Using a forward model to calculate displacement and then comparing the results to GPS observations, Pollitz (2005) was able to determine the range of possible Earth structures that best fit the data, finding upper-mantle viscosities of 1×10^{17} (transient) and 2.5×10^{18} Pa s (steady state).

The approach used by the aforementioned studies to solve for a value of mantle viscosity does not consider the environmental conditions such as temperature, pressure, grain size or water content. Freed *et al.* (2010) took a different approach by

using a laboratory-derived steady-state power-law rheology, which is a function of the different environmental parameters, and investigated whether it could explain the GPS-observed post-seismic response to the 1999, magnitude 7.1, Hector Mine earthquake in California. They found that they could not replicate the observed surface displacement from 7 years of GPS data at 55 locations in the far field (>50 km from the earthquake rupture) with the steady-state flow law and suggested that a transient phase is also required: that is, where deformation is enhanced immediately after the earthquake compared to the steady-state response.

Freed *et al.* (2012) developed this idea by formulating a constitutive relationship combining transient and steady-state flow, which is a function of the environmental parameters, to predict the spatial and temporal post-seismic viscoelastic deformation. They found that they could fit the GPS data with a transient phase of approximately 1 year and with a viscosity around 10 times lower than the steady-state viscosity. Because this flow law is a function of ambient conditions, in theory it can be applied to any earthquake in any region so long as the environmental parameters are known.

Results for Antarctica

Antarctica lies within the Antarctic Plate and comprises two geologically distinct regions: the old cratons of East Antarctica and the active rift system of West Antarctica. The majority of the Antarctic Plate is connected to the surrounding tectonic plates by spreading rifts (Reading 2007). The northern Antarctic Peninsula, lying close to the plate boundary, is tectonically complex as discussed in the earlier subsection on 'GIA model results and inferences of mantle structure'. The active tectonic setting of the Antarctic Peninsula means that it is likely to have a lower mantle viscosity than other regions of Antarctica, as discussed in the 'GIA model results and inferences of mantle structure' subsection (Ivins *et al.* 2011; Nield *et al.* 2014), which may result in a more pronounced post-seismic response.

Seismicity generally occurs at a low level around the plate boundaries of the Antarctic Plate, except for two regions. Earthquakes with a magnitude greater than 7 have been recorded at the plate boundary between the Antarctic Plate and the Scotia Plate (Fig. 9); two strike-slip earthquakes have occurred at this location since 2003 (magnitude 7.6 in 2003 and magnitude 7.7 in 2013: Ye *et al.* 2014). The Macquarie Ridge Complex, where the Antarctic Plate meets the Australian and Pacific plates (Fig. 9), has also experienced three earthquakes of magnitude 7.7 or greater in the past *c.* 100 years (Watson *et al.* 2010).

Continental Antarctica was once thought to be aseismic (i.e. very few earthquakes occurred in this region) and it was not until the 1980s that an earthquake was definitively shown to have occurred here (Adams *et al.* 1985; Adams and Akoto 1986). The magnitude 4.5 earthquake occurred on 4 November 1982, *c.* 1200 km from the coast of Dronning Maud Land, and was detected by five seismic stations. Despite this confirmation of the existence of intraplate earthquakes, the continent of Antarctica was still thought to experience fewer intraplate earthquakes than other equivalent regions possibly due to the weight of the overlying ice sheet (Johnston 1987). However, the lack of recorded seismic activity was, in fact, due to the small number of seismic stations operating in this region rather than the absence of earthquakes. Following the installation of seismographs in East Antarctica during the International Polar Year, Lough *et al.* (2018) showed that during 2009 intraplate earthquakes occurred at the same frequency and magnitude as in other cratons. Given the lack of recorded earthquakes, it is no surprise that the study of post-seismic deformation in Antarctica is not well established compared with other regions of the world.

Earthquakes in continental Antarctica occur in several regions such as the Transantarctic Mountains and around the coastline (Reading 2007). The most notable intraplate earthquake occurred near Balleny Islands, an area of high seismicity close to the plate boundary south of New Zealand. This magnitude 8.1 earthquake occurred on 25 March 1998, 500 km from the Antarctic coastline (Nettles *et al.* 1999; Henry *et al.* 2000) and is the subject of the only published study on post-seismic deformation of Antarctica (King and Santamaría-Gómez 2016).

King and Santamaría-Gómez (2016) sought to place constraints on the properties of the Antarctic mantle by constraining a model of post-seismic viscoelastic deformation using geodetic measurements. They estimated initial coseismic displacement from continuous GPS observations made at the Dumont d'Urville Station located 600 km from the 1998

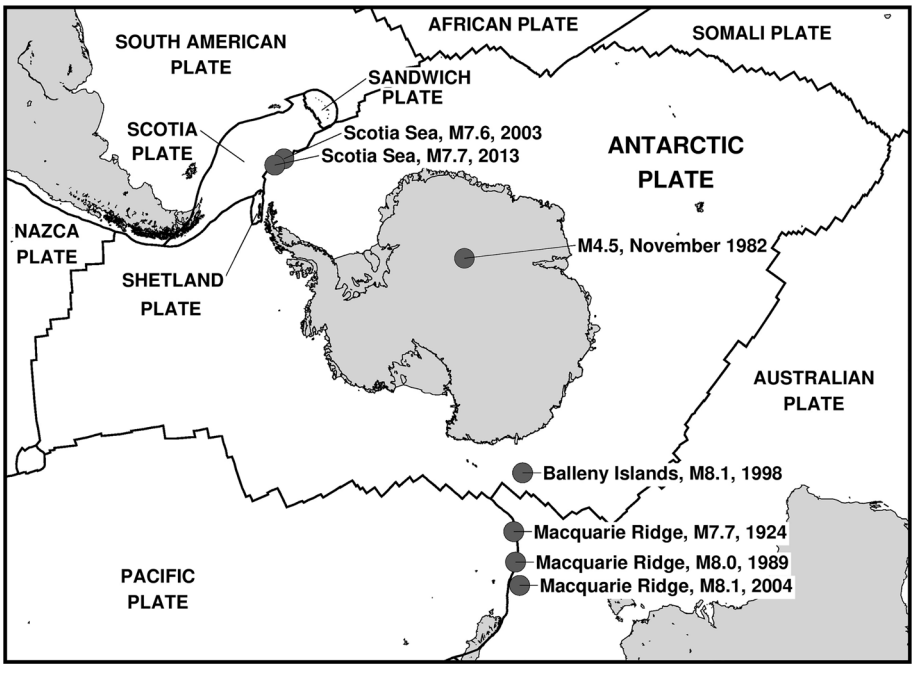

Fig. 9. Map of Antarctica with plate boundaries and the location of earthquakes mentioned in the text.

earthquake, and used this displacement to tune fault parameters such as geometry and slip magnitude. The resulting fault parameters provided input to a model of post-seismic viscoelastic deformation. The authors also considered the magnitude 8.1 2004 earthquake that occurred at the Macquarie Ridge (Fig. 9). Whilst the coseismic offset from this earthquake is small (submillimetre) at all Antarctic sites, there may be a post-seismic deformation signal present at Dumont d'Urville, as indicated in the GPS time series.

They used the VISCO1D program with a suite of layered, spherically symmetrical Earth models to predict post-seismic deformation from both the 1998 and 2004 earthquakes, and compared model outputs to bedrock coordinate time series from continuous GPS, campaign GPS, and Doppler Orbitography and Radiopositioning Integrated by Satellite (DORIS) data from the Dumont d'Urville Station. The Earth models consisted of a purely elastic lithosphere, and asthenosphere and upper mantle layers with biviscous Burger's rheology that has a transient viscosity one order of magnitude lower than the steady-state viscosity. The thickness of each layer was varied but the base of the upper mantle was fixed at a depth of 670 km.

When comparing modelled with observed horizontal motions, the authors found a best-fitting Earth model with a 90 km-thick lithosphere, a 130 km-thick asthenosphere with steady-state viscosity of 1.2×10^{19} Pa s and an upper-mantle steady-state viscosity of 1.4×10^{19} Pa s (at a depth of between 220 and 670 km). However, King and Santamaría-Gómez (2016) could not find any Earth structure that satisfactorily reproduced both the observed vertical deformation and the horizontal deformation simultaneously, and suggested that using a 3D Earth structure may solve at least part of this issue. This result is important because it may be indicative of the presence of lateral variations in the Earth structure, particularly a contrast between oceanic and continental mantle viscosity, as has also been hypothesized from isotopic studies of volcanic rock in this region (Panter *et al.* 2018). The study of post-seismic deformation clearly has the potential to constrain mantle structure in Antarctica.

Conclusions and future work

In this section, the main conclusions of glacial isostatic adjustment (GIA) and post-seismic studies in Antarctica are summarized and possible future research is outlined in three sections: the contribution of GIA and post-seismic deformation to knowledge of the mantle, future research in the field of GIA, and future research in the field of post-seismic deformation.

GIA is mainly due to the shrinking of the ice sheet since the last glacial maximum (LGM: *c.* 20 kyr ago). The total volume of ice that disappeared was for a long time mainly constrained by assigning to the Antarctic Ice Sheet the amount of ice needed to reconcile the contribution to the sea level from the known land ice masses on the other continents with the total global sea-level change. This resulted in a large ice loss from Antarctica of 25 m sea-level equivalent (SLE). Relying on an indirect constraint from the global sea level was necessary due to the lack of direct and indirect evidence from Antarctica itself. This situation has now improved, and, more recently, geodetic and seismic data and improved ice-dynamics models have led to lower estimates of 5–15 m of global SLE. Melting occurred asynchronously, mostly starting at *c.* 15 ka BP. Most of the ice disappeared from the Ross and Filchner-Ronne ice shelf areas. For East Antarctica, some models show an increase in ice thickness since the LGM. During the late Holocene, readvance occurred in some places, possibly aided by rebound due to GIA following a retreating ice sheet. Closer to present, melting after the Little Ice Age occurred in parts of West Antarctica such as the Amundsen Sea Embayment.

Post-seismic deformation occurs due to plate motion that generates large (magnitude >7) earthquakes. Earthquakes of sufficient magnitude occurred at plate margins north of the Antarctic Peninsula and south of New Zealand. Data about this phenomenon have been lacking in the region as insufficient GPS receivers were in place to detect most of the large earthquakes. A 1998 earthquake was both large enough and sufficiently covered by GPS measurements for post-seismic motion to be detected at the level of 2 mm a^{-1}.

GNSS receivers measure 3D deformation and show uplift of centimetres per year in the Amundsen Sea sector. Smaller velocities in the range of millimetres per year in areas such as the Filchner-Ronne and Ross ice shelves can be related to GIA. Horizontal velocities are harder to relate to GIA models, except in the Amundsen Sea sector. GIA is recorded in palaeosea-level observations at a dozen locations near the Antarctic coastline, showing tens of metres of uplift. Data in East Antarctica are quite sparse relative to West Antarctica, and data from both are infrequent relative to other continents. In general, continental-scale GIA models for Antarctica are relatively unconstrained but GNSS data help to make regional GIA studies more constrained.

GIA and post-seismic deformation use similar geophysical models. These require elastic and viscous parameters as input. In most GIA models, a Maxwell rheology is used where elastic deformation is followed by steady-state viscous deformation. In post-seismic models, a fast, short-term viscosity is found to be necessary, which leads to a Burger's rheology with a short-term and a long-term viscous element. GIA models estimate an average viscosity of 10^{20}–10^{21} Pa s for the Antarctic upper mantle. Regional studies show low viscosity (<10^{18} Pa s) in the northern Antarctic Peninsula, increasing to 10^{20} Pa s in the southern Antarctic Peninsula. This increasing viscosity agrees with subduction that terminates from south to north. The post-seismic deformation following the 1998 earthquake near the Balleny Islands that has been detected and compared to model outputs leads to a best-fitting viscosity of 1.2×10^{19} Pa s in the shallow, and 1.4×10^{19} Pa s in the deeper upper mantle, similar to GIA-based estimates for the Antarctic Peninsula. Low viscosity (4×10^{18} Pa s) is also found in the Amundsen Sea sector, an area with geologically recent rifting and volcanism. These viscosity inferences agree with maps of 3D viscosity created from seismic velocity anomalies that are converted to viscosity anomalies. In fact, the argument should be reversed: the uncertainty in 3D viscosity maps can be considered so high that regional studies (both geophysical and geological) are needed to provide a constraint on (parts of) such viscosity maps.

The timing of the Earth's response to changes in loading is driven by the local mantle viscosity. Low viscosities (10^{17}–10^{18} Pa s) in the Antarctic upper mantle can be translated into a relaxation time in the years to decades range, much faster than in classical GIA areas, but similar to GIA in areas near rifts or subduction such as Iceland, Alaska and Patagonia. The low viscosity also guarantees a strong influence on the ice sheets in Antarctica by changing the local sea level: post-glacial uplift raises land ice from the sea and reduces the ice–ocean contact area and, hence, melt. The instability of an inward-moving grounding line in combination with topography that deepens inland can be somewhat reduced by GIA. This process can be accounted for with schematic models that require a single relaxation time as a parameter, or with a viscoelastic half-space model, or full-fledged 3D GIA simulations. Accounting for this feedback with the most accurate model is shown to affect the total volume of the LGM Antarctic Ice Sheet by 1–3 m SLE and to affect the grounding-line position by hundreds of kilometres in the marine-grounded ice sheets in the Ross and Weddell seas.

Outlook on contribution of GIA and post-seismic deformation to knowledge of the mantle

Simulations of GIA and post-seismic deformation depend on mantle viscosity. However, their different sensitivities and timescales mean that results from one study are not directly comparable to mantle viscosity structure in another study because different regions and timescales are sampled. For example, even if the Earth structure is identical across different simulations, the effective lithosphere for shorter loading phenomena is thicker because the mantle below has had less time to adjust viscously (Nield *et al.* 2018; Lau *et al.* 2021). A step forward is the use of seismic models, flow laws, geological observations and material parameters to create mantle profiles that can be used and tested in different geodynamic studies, and where lithosphere thickness is implicit in the 3D viscosity distribution.

The use of seismic velocity anomalies as a proxy for viscosity variations raises the issues of accuracy of conversion of seismic velocity anomalies to temperature and viscosity. The question whether temperature or composition explains a seismic velocity anomaly cannot be answered *a priori* and requires other information that could come from xenoliths, which record grain size, water content and chemistry from which pressure and temperature conditions can be calculated that are relevant in the flow of the main mantle material olivine (Martin 2021, this volume). These show heterogeneity on all scales. There is evidence in Antarctica for the occurrence of large grain sizes that would increase viscosity but also for the presence of water in mantle rocks, which has a weakening effect. Besides isolated findings of mantle rocks, the mantle structure can also be elucidated by the geological history and the tectonic link to surrounding continents. The observed high heat flow in West Antarctica could provide a constraint on thermal modelling of the mantle, although heat-flow measurements are sparse (Burton-Johnson *et al.* 2020; Pappa and Ebbing 2021, this volume). Gravity-field variations provide a strong test of mantle structure. Thermal anomalies as used in geodynamic models can be converted to density and gravity anomalies with less uncertainty than in the conversion to viscosity. The resulting gravity-field variations must match the observed gravity, which, for the long wavelengths that contain the mantle signal, is known with high accuracy (Pappa and Ebbing 2021, this volume).

The translation from material parameters and conditions of the mantle to viscosity requires flow laws (i.e. relations between stress and strain rate). Experiments show that even for the same material, the effective viscosity is different for different processes because the bedrock relaxation is not in steady state (i.e. transient rheology) or because one of the mantle-flow mechanisms is strongly dependent on stress (i.e. dislocation creep). For the above reasons, Lau *et al.* (2021) argued that the standard description of viscosity should be replaced by frequency dependence of viscosity, which would lead to a different effective viscosity for LGM ice-sheet unloading than for the recent changes in the Antarctic Peninsula. It will be a large challenge to create a framework that can unify geological observations, the seismic measurements with the obtained viscosity in West Antarctica and the average viscosities found in 1D GIA studies.

The emerging area of post-seismic deformation research has the potential to reveal information about the mantle in Antarctica, providing complementary results to GIA as the processes span different timescales and affect different regions of the mantle. Post-seismic deformation occurs over years to decades, predominantly in the shallow upper mantle, whereas GIA may occur over hundreds to thousands of years invoking a response at much greater depths. There are a few select regions (such as the northern Antarctic Peninsula) where the timescale of these processes overlaps, presenting an opportunity to use post-seismic deformation and GIA to constrain the lithosphere and mantle.

Generalizing this idea further, the same Earth model should be applied for regional recent loading and continent-wide LGM ice sheets, post-seismic deformation and mantle convection, and be compared to the geophysical, geological and geodetic observations of these processes. In particular, the horizontal velocities hold promise because of their different sensitivities (Hermans *et al.* 2018) and availabilities near areas of viscosity contrast (Konfal *et al.* 2018). Integrating results from regional studies and other processes in 3D viscosity maps is not straightforward; it is not known *a priori* how the GIA process samples the 3D Earth (Powell *et al.* 2020). Sensitivity studies can enlighten the depth sensitivity, as well as the relevant horizontal extent, so that the regional GIA or post-seismic studies can provide unbiased anchor points for 3D effective viscosity models (see table 6 in Ivins *et al.* 2021, this volume). Integrating more geodynamic processes and their observations provide more constraints that can be assimilated. This complicates and lengthens simulations and interpretations but in the end is the best way to unveil the true Earth structure.

Future research on GIA in Antarctica

The construction of the ice history is the main uncertainty in GIA model predictions. Ice dynamics cannot yet provide an ice-sheet history with large confidence: for example, knowledge of subglacial processes and interaction between ice and ocean requires improvement (Siegert and Golledge 2022). In addition, more efforts are necessary to estimate ice-thickness variations in the last millennium. It has been demonstrated that several regions in West Antarctica, and also at the coast of East Antarctica, have lower upper-mantle viscosity, responding on a timescale of years to hundreds of years, which means their uplift is sensitive to the late Holocene or even the last decades of ice-sheet evolution. Furthermore, there is evidence for grounding-line readvance, which complicates the picture in most GIA models of monotonous retreat (Kingslake *et al.* 2018; Simms *et al.* 2021). Deepening and integrating this knowledge with the last LGM maximum ice history will be a major step forward for GIA modelling. At the same time, improvements in the physical description of ice-sheet behaviour will go hand in hand with improved predictions for future scenarios of decline of the Antarctic Ice Sheet.

The picture of the Antarctic mantle that emerged from seismic data and mantle xenolith and volcanic rock studies shows variations in mantle structure from West Antarctica to East Antarctica and within subregions of Antarctica such as the Antarctic Peninsula. However, there are uncertainties in the seismic models themselves (Wiens *et al.* 2021, this volume), as well as in the conversion to viscosity (Ivins *et al.* 2021, this volume). Moreover, seismic data have limited resolution in the lower mantle, where a significant part of the GIA sensitivity could reside. Global models show small anomalies in the lower mantle but Lloyd *et al.* (2020) showed an anomaly below Marie Bird Land that continues into the lower mantle (Wiens *et al.* 2021, this volume). Improved lower-mantle seismic velocity anomalies in other regions will lead to improved GIA predictions. Further constraints on viscosity are necessary. If flow laws are used to derive effective viscosity, Antarctica water content and grain size are usually the largest uncertainties (van der Wal *et al.* 2015; King *et al.* 2016; Blank *et al.* 2021). Water content, however, can be measured in xenoliths or igneous olivine from which trends on spatial variations in water content within Antarctica could be deduced

that could be applied in GIA models (Martin 2021, this volume).

With the current knowledge of the distinct domains in East and West Antarctica, the few studies that interpreted sea-level records before the LGM could be revisited. On such time scales, infill of sediments can form a considerable load. Sediment deposition mapped offshore also offers constraints on where erosion occurred and, hence, where ice-sheet flow originated (Naish *et al.* 2022). The latter could require coupling between ice-sheet erosion models such as done by Jamieson *et al.* (2010) to model the evolution of subglacial topography. On longer timescales, the evolution of the topography due to sedimentation and vertical motion due to dynamic topography and tectonics should also be taken into account, as the topography controls ice-sheet flow (Whitehouse *et al.* 2019; Colleoni *et al.* 2022).

All of the above play a large role in West Antarctica where most of the rapid ice melt occurs, and which sees low viscosity and large variations in tectonic regimes. However, East Antarctica holds most of the freshwater and there are several regions in East Antarctica where glaciers are thinning fast (Rignot 2006). East Antarctica is much less covered by seismic or geodetic data, for obvious logistic reasons. This lack of knowledge presents considerable uncertainty in understanding the evolution and future of the Antarctica Ice Sheet and associated sea-level changes. Therefore, improved data coverage in East Antarctica is desirable, albeit challenging and costly.

Future research on post-seismic deformation in Antarctica

The study of post-seismic viscoelastic deformation in Antarctica is still in its early stages but King and Santamaría-Gómez (2016) have shown that the continent is, or has been, affected by widespread deformation following the 1998 earthquake near the Balleny Islands. This demonstrates the potential for future post-seismic studies to reveal information about Antarctica's mantle, particularly in terms of 3D Earth properties that may be needed to explain observations. Future studies will be likely to focus on other large earthquakes, particularly those that have occurred during the era of geodetic observation such as the 2003 and 2013 Scotia Sea earthquakes that occurred close to the northern Antarctic Peninsula. Furthermore, the possibility of a transient phase should be investigated where the mantle responds more quickly over a shorter timescale immediately following the sudden change in stress, as has proved necessary to explain the response to earthquakes in other regions (Pollitz 2005; Freed *et al.* 2012).

High-quality and plentiful geodetic data are key to being able to constrain Earth properties from post-seismic deformation, as studies have done for other regions of the world. With around 75 continuous GPS stations operating across Antarctica, the situation has vastly improved from the sparse arrays in operation at the time of the 1998 Balleny Islands and 2003 Scotia Sea earthquakes. This shows the importance of maintaining and building on existing networks, such as the Antarctic-Network (A-NET) project (Wilson *et al.* 2020), which will provide more observations to constrain models. Furthermore, improved models of post-seismic viscoelastic deformation, which include lateral variations in Earth properties, will be needed in regions where traditional 1D Earth structures (10^{20}–10^{21} Pa s upper-mantle viscosity: see the subsection on 'GIA model results and inferences of mantle structure') cannot match observations in all components of deformation.

Acknowledgements The authors thank the two reviewers for their comments, which helped to improve the manuscript, and Pippa Whitehouse for providing data and information on the W12 ice model. Several of the figures used the mapping tools of Greene *et al.* (2017), the colour maps of Crameri (2018) and the Generic Mapping Tools (Wessel *et al.* 2019).

Competing interest The authors declare that they have no known competing financial interests or personal relationships that could have appeared to influence the work reported in this chapter.

Author contributions **WVDW**: writing – original draft (lead), writing – review & editing (equal); **VB**: writing – original draft (supporting), writing – review & editing (equal); **GN**: writing – original draft (supporting), writing – review & editing (equal); **CVC**: writing – original draft (supporting), writing – review & editing (equal).

Funding The work is partially funded by projects GOCE + Antarctica and 3-D Earth funded by the European Space Agency (ESA) as a Support to Science Element.

Data availability Data sharing is not applicable to this article as no datasets were generated or analysed during the current study.

References

Adams, R.D. and Akoto, A.M. 1986. Earthquakes in continental Antarctica. *Journal of Geodynamics*, **6**, 263–270, https://doi.org/10.1016/0264-3707(86)90043-8

Adams, R.D., Hughes, A.A. and Zhang, B.M. 1985. A confirmed earthquake in continental Antarctica. *Geophysical Journal International*, **81**, 489–492, https://doi.org/10.1111/j.1365-246X.1985.tb06416.x

Adhikari, S., Ivins, E.R., Larour, E., Seroussi, H., Morlighem, M. and Nowicki, S. 2014. Future Antarctic bed topography and its implications for ice sheet dynamics. *Solid Earth*, **5**, 569–584, https://doi.org/10.5194/se-5-569-2014

Agata, R., Barbot, S.D. *et al.* 2019. Rapid mantle flow with power-law creep explains deformation after the 2011 Tohoku mega-quake. *Nature Communications*, **10**, 1385, https://doi.org/10.1038/s41467-019-08984-7

Albrecht, T. 2019. PISM parameter ensemble analysis of Antarctic Ice Sheet glacial cycle simulations, PANGAEA, https://doi.org/10.1594/PANGAEA.909728

Albrecht, T., Winkelmann, R. and Levermann, A. 2020*a*. Glacial-cycle simulations of the Antarctic Ice Sheet with the Parallel Ice Sheet Model (PISM) – Part 1: Boundary conditions and climatic forcing. *The Cryosphere*, **14**, 599–632, https://doi.org/10.5194/tc-14-599-2020

Albrecht, T., Winkelmann, R. and Levermann, A. 2020*b*. Glacial-cycle simulations of the Antarctic Ice Sheet with the Parallel Ice Sheet Model (PISM) – Part 2: Parameter ensemble analysis. *The Cryosphere*, **14**, 633–656, https://doi.org/10.5194/tc-14-633-2020

An, M., Wiens, D.A. *et al.* 2015. Temperature, lithosphere-asthenosphere boundary, and heat flux beneath the Antarctic Plate inferred from seismic velocities. *Journal of Geophysical Research: Solid Earth*, **120**, 8720–8742, https://doi.org/10.1002/2015JB011917

Argus, D.F., Peltier, W.R., Drummond, R. and Moore, A.W. 2014. The Antarctica component of postglacial rebound model ICE-6G_C (VM5a) based on GPS positioning, exposure age dating of ice thicknesses, and relative sea level histories. *Geophysical Journal International*, **198**, 537–563, https://doi.org/10.1093/gji/ggu140

Arndt, J.E., Schenke, H.W. *et al.* 2013. The International Bathymetric Chart of the Southern Ocean (IBCSO) Version 1.0 – A new bathymetric compilation covering circum-Antarctic waters. *Geophysical Research Letters*, **40**, 3111–3117, https://doi.org/10.1002/grl.50413

Bagge, M., Klemann, V., Steinberger, B., Latinović, M. and Thomas, M. 2021. Glacial-isostatic adjustment models using geodynamically constrained 3D earth structures. *Geochemistry, Geophysics, Geosystems*, **22**, e2021GC009853, https://doi.org/10.1029/2021GC009853

Bamber, J.L., Riva, R.E.M., Vermeersen, B.L.A. and LeBrocq, A.M. 2009. Reassessment of the potential sea-level rise from a collapse of the West Antarctic Ice Sheet. *Science*, **324**, 901–903, https://doi.org/10.1126/science.1169335

Barker, D.H.N. and Austin, J.A. Jr 1998. Rift propagation, detachment faulting, and associated magmatism in Bransfield Strait, Antarctic Peninsula. *Journal of Geophysical Research: Solid Earth*, **103**, 24017–24043, https://doi.org/10.1029/98JB01117

Barker, P. 1982. The Cenozoic subduction history of the Pacific margin of the Antarctic Peninsula: ridge crest–trench interactions. *Journal of the Geological Society, London*, **139**, 787–801, https://doi.org/10.1144/gsjgs.139.6.0787

Barletta, V.R., Bevis, M. *et al*. 2018. Observed rapid bedrock uplift in Amundsen Sea Embayment promotes ice-sheet stability. *Science*, **360**, 1335–1339, https://doi.org/10.1126/science.aao1447

Barnhoorn, A., van der Wal, W., Vermeersen, B.L.A. and Drury, M.R. 2011. Lateral, radial, and temporal variations in upper mantle viscosity and rheology under Scandinavia. *Geochemistry, Geophysics, Geosystems*, **12**, Q01007, https://doi.org/10.1029/2010GC003290

Bassett, S.E., Milne, G.A., Bentley, M.J. and Huybrechts, P. 2007. Modelling Antarctic sea-level data to explore the possibility of a dominant Antarctic contribution to meltwater pulse IA. *Quaternary Science Reviews*, **26**, 2113–2127, https://doi.org/10.1016/j.quascirev.2007.06.011

Bentley, M.J. 1999. Volume of Antarctic Ice at the Last Glacial Maximum, and its impact on global sea level change. *Quaternary Science Reviews*, **18**, 1569–1595, https://doi.org/10.1016/S0277-3791(98)00118-8

Bentley, M.J. and Anderson, J.B. 1998. Glacial and marine geological evidence for the ice sheet configuration in the Weddell Sea–Antarctic Peninsula region during the Last Glacial Maximum. *Antarctic Science*, **10**, 309–325, https://doi.org/10.1017/S0954102098000388

Bentley, M.J., Hodgson, D.A., Smith, J.A. and Cox, N.J. 2005. Relative sea level curves for the South Shetland Islands and Marguerite Bay, Antarctic Peninsula. *Quaternary Science Reviews*, **24**, 1203–1216, https://doi.org/10.1016/j.quascirev.2004.10.004

Bentley, M.J., Ó Cofaigh, C. *et al*. 2014. A community-based geological reconstruction of Antarctic Ice Sheet deglaciation since the Last Glacial Maximum. *Quaternary Science Reviews*, **100**, 1–9, https://doi.org/10.1016/j.quascirev.2014.06.025

Berg, J.H., Moscati, R.J. and Herz, D.L. 1989. A petrologic geotherm from a continental rift in Antarctica. *Earth and Planetary Science Letters*, **93**, 98–108, https://doi.org/10.1016/0012-821X(89)90187-8

Bevis, M., Wahr, J. *et al*. 2012. Bedrock displacements in Greenland manifest ice mass variations, climate cycles and climate change. *Proceedings of the National Academy of Sciences of the United States of America*, **109**, 11 944–11 948, https://doi.org/10.1073/pnas.1204664109

Bills, B.G. and James, T.S. 1996. Late Quaternary variations in relative sea level due to glacial cycle polar wander. *Geophysical Research Letters*, **23**, 3023–3026, https://doi.org/10.1029/96GL02886

Blank, B., Barletta, V., Hu, H., Pappa, F. and van der Wal, W. 2021. Effect of lateral and stress-dependent viscosity variations on GIA induced uplift rates in the Amundsen Sea embayment. *Geochemistry, Geophysics, Geosystems*, **22**, e2021GC009807, https://doi.org/10.1029/2021GC009807

Bradley, S.L., Hindmarsh, R.C.A., Whitehouse, P.L., Bentley, M.J. and King, M.A. 2015. Low post-glacial rebound rates in the Weddell Sea due to Late Holocene ice-sheet readvance. *Earth and Planetary Science Letters*, **413**, 79–89, https://doi.org/10.1016/j.epsl.2014.12.039

Brandes, C., Steffen, H., Steffen, R. and Wu, P. 2015. Intraplate seismicity in northern Central Europe is induced by the last glaciation. *Geology*, **43**, 611–614, https://doi.org/10.1130/G36710.1

Bredow, E., Steinberger, B., Gassmöller, R. and Dannberg, J. 2022. Mantle convection and possible mantle plumes beneath Antarctica – insights from geodynamic models and implications for topography. *Geological Society, London, Memoirs*, **56**, https://doi.org/10.1144/M56-2020-2

Briggs, R.D. and Tarasov, L. 2013. How to evaluate model-derived deglaciation chronologies: a case study using Antarctica. *Quaternary Science Reviews*, **63**, 109–127, https://doi.org/10.1016/j.quascirev.2012.11.021

Briggs, R.D., Pollard, D. and Tarasov, L. 2014. A data-constrained large ensemble analysis of Antarctic evolution since the Eemian. *Quaternary Science Reviews*, **103**, 91–115, https://doi.org/10.1016/j.quascirev.2014.09.003

Broerse, D.B.T., Vermeersen, L.L.A., Riva, R.E.M. and van der Wal, W. 2011. Ocean contribution to co-seismic crustal deformation and geoid anomalies: Application to the 2004 December 26 Sumatra–Andaman earthquake. *Earth and Planetary Science Letters*, **305**, 341–349, https://doi.org/10.1016/j.epsl.2011.03.011

Brook, E.J., Kurz, M.D., Ackert, R.P., Denton, G.H., Brown, E.T., Raisbeck, G.M. and Yiou, F. 1993. Chronology of Taylor Glacier advances in Arena Valley, Antarctica, using *in situ* cosmogenic ^{3}He and ^{10}Be. *Quaternary Research*, **39**, 11–23, https://doi.org/10.1006/qres.1993.1002

Bueler, E., Lingle, C.S. and Brown, J. 2007. Fast computation of a viscoelastic deformable Earth model for ice-sheet simulations. *Annals of Glaciology*, **46**, 97–105, https://doi.org/10.3189/172756407782871567

Burton-Johnson, A., Dziadek, R. *et al*. 2020. *Antarctic Geothermal Heat Flow: Future Research Directions*. SCAR-SERCE White Paper. Scientific Committee on Antarctic Research (SCAR), Cambridge, UK, https://scar.org/scar-library/search/science-4/research-programmes/serce/5454-scar-serce-white-paper-on-antarctic-geothermal-heat-flow/

Caron, L. and Ivins, E.R. 2020. A baseline Antarctic GIA correction for space gravimetry. *Earth and Planetary Science Letters*, **531**, 115957, https://doi.org/10.1016/j.epsl.2019.115957

Caron, L., Métivier, L., Greff-Lefftz, M., Fleitout, L. and Rouby, H. 2017. Inverting Glacial Isostatic Adjustment signal using Bayesian framework and two linearly relaxing rheologies. *Geophysical Journal International*, **209**, 1126–1147, https://doi.org/10.1093/gji/ggx083

Cathles, L.M. 1975. *Viscosity of the Earth's Mantle*. Princeton Legacy Library, Princeton, NJ.

Christensen, U. 1984. Convection with pressure- and temperature-dependent non-Newtonian rheology. *Geophysical Journal International*, **77**, 343–384, https://doi.org/10.1111/j.1365-246X.1984.tb01939.x

Clark, J.A. and Lingle, C.S. 1979. Predicted relative sea-level changes (18,000 years B.P. to present) caused by late-glacial retreat of the Antarctic Ice Sheet. *Quaternary Research*, **11**, 279–298, https://doi.org/10.1016/0033-5894(79)90076-0

Clark, J.A., Farrell, W.E. and Peltier, W.R. 1978. Global changes in postglacial sea level: A numerical calculation. *Quaternary Research*, **9**, 265–287, https://doi.org/10.1016/0033-5894(78)90033-9

Clark, P.U. and Tarasov, L. 2014. Closing the sea level budget at the Last Glacial Maximum. *Proceedings of the National Academy of Sciences of the United States of America*, **111**, 15 861–15 862, https://doi.org/10.1073/pnas.1418970111

Colleoni, F., De Santis, L. *et al*. 2018. Spatio-temporal variability of processes across Antarctic ice-bed–ocean interfaces. *Nature Communications*, **9**, 2289, https://doi.org/10.1038/s41467-018-04583-0

Colleoni, F., De Santis, L. *et al*. 2022. Past Antarctic ice sheet dynamics (PAIS) and implications for future sea-level change. *In*: Florindo, F., Siegart, M., De Santis, L. and Naish, T. (eds) *Antarctic Climate Evolution*. Elsevier, 689–768, https://doi.org/10.1016/B978-0-12-819109-5.00010-4

Coltorti, M., Bonadiman, C., Casetta, F., Faccini, B., Giacomoni, P.P., Pelorosso, B. and Perinelli, C. 2021. Nature and evolution of the northern Victoria Land lithospheric mantle (Antarctica) as revealed by ultramafic xenoliths. *Geological Society, London, Memoirs*, **56**, https://doi.org/10.1144/M56-2020-11

Coulon, V., Bulthuis, K., Whitehouse, P.L., Sun, S., Haubner, K., Zipf, L. and Pattyn, F. 2021. Contrasting response of West and East Antarctic ice sheets to glacial isostatic adjustment. *Journal of Geophysical Research: Earth Surface*, **126**, e2020JF006003, https://doi.org/10.1029/2020JF006003

Crameri, F. 2018. Geodynamic diagnostics, scientific visualisation and StagLab 3.0. *Geoscientific Model Development*, **11**, 2541–2562, https://doi.org/10.5194/gmd-11-2541-2018

Crawford, O., Al-Attar, D., Tromp, J. and Mitrovica, J.X. 2017. Forward and inverse modelling of post-seismic deformation. *Geophysical Journal International*, **208**, 845–876, https://doi.org/10.1093/gji/ggw414

Crawford, O., Al-Attar, D., Tromp, J., Mitrovica, J.X., Austermann, J. and Lau, H.C.P. 2018. Quantifying the sensitivity of post-glacial sea level change to laterally varying viscosity. *Geophysical Journal International*, **214**, 1324–1363, https://doi.org/10.1093/gji/ggy184

Davies, B.J., Hambrey, M.J., Smellie, J.L., Carrivick, J.L. and Glasser, N.F. 2012. Antarctic Peninsula Ice Sheet evolution during the Cenozoic Era. *Quaternary Science Reviews*, **31**, 30–66, https://doi.org/10.1016/j.quascirev.2011.10.012

Davis, B. 2020. Cosmogenic nuclide dating. AntarcticGlaciers.org, http://www.antarcticglaciers.org/glacial-geology/dating-glacial-sediments-2/cosmogenic_nuclide_datin/ [last accessed April 2022].

de Boer, B., Stocchi, P. and van de Wal, R.S.W. 2014. A fully coupled 3-D ice-sheet–sea-level model: algorithm and applications. *Geoscientific Model Development*, **7**, 2141–2156, https://doi.org/10.5194/gmd-7-2141-2014

DeConto, R.M., Pollard, D. *et al*. 2021. The Paris Climate Agreement and future sea-level rise from Antarctica. *Nature*, **593**, 83–89, https://doi.org/10.1038/s41586-021-03427-0

Denton, G.H. and Hughes, T.J. 2002. Reconstructing the Antarctic Ice Sheet at the Last Glacial Maximum. *Quaternary Science Reviews*, **21**, 193–202, https://doi.org/10.1016/S0277-3791(01)00090-7

Denton, G.H., Bockheim, J.G., Rutford, R.H., Andersen, B.G., Webers, G.F., Craddock, C. and Splettstoesser, J.F. 1992. Glacial history of the Ellsworth Mountains, West Antarctica. *Geological Society of America Memoirs*, **170**, 403–432, https://doi.org/10.1130/MEM170-p403

Dietrich, R., Ivins, E.R., Casassa, G., Lange, H., Wendt, J. and Fritsche, M. 2010. Rapid crustal uplift in Patagonia due to enhanced ice loss. *Earth and Planetary Science Letters*, **289**, 22–29, https://doi.org/10.1016/j.epsl.2009.10.021

Donda, F., O'Brien, P.E., De Santis, L., Rebesco, M. and Brancolini, G. 2008. Mass wasting processes in the Western Wilkes Land margin: Possible implications for East Antarctic glacial history. *Palaeogeography, Palaeoclimatology, Palaeoecology*, **260**, 77–91, https://doi.org/10.1016/j.palaeo.2007.08.008

Eagles, G., Gohl, K. and Larter, R.D. 2004. High-resolution animated tectonic reconstruction of the South Pacific and West Antarctic Margin. *Geochemistry, Geophysics, Geosystems*, **5**, Q07002, https://doi.org/10.1029/2003GC000657

Ekman, M. 1991. A concise history of postglacial land uplift research (from its beginning to 1950). *Terra Nova*, **3**, 358–365, https://doi.org/10.1111/j.1365-3121.1991.tb00163.x

Ekman, M. 2013. *An Investigation of Celsius' Pioneering Determination of the Fennoscandian Land Uplift Rate, and of His Mean Sea Level Mark*. Small Publications in Historical Geophysics, **25**.

Farrell, W.E. and Clark, J.A. 1976. On postglacial sea level. *Geophysical Journal International*, **46**, 647–667, https://doi.org/10.1111/j.1365-246X.1976.tb01252.x

Faul, U. and Jackson, I. 2015. Transient creep and strain energy dissipation: An experimental perspective. *Annual Review of Earth and Planetary Sciences*, **43**, 541–569, https://doi.org/10.1146/annurev-earth-060313-054732

Feng, G., Hetland, E.A., Ding, X., Li, Z. and Zhang, L. 2010. Coseismic fault slip of the 2008 M_w 7.9 Wenchuan earthquake estimated from InSAR and GPS measurements. *Geophysical Research Letters*, **37**, L01302, https://doi.org/10.1029/2009GL041213

Findley, W.N., Lai, J.S. and Onaran, K. 1976. *Creep and Relaxation of Nonlinear Viscoelastic Materials: With an Introduction to Linear Viscoelasticity*. North Holland, Amsterdam.

Freed, A.M., Herring, T. and Bürgmann, R. 2010. Steady-state laboratory flow laws alone fail to explain postseismic observations. *Earth and Planetary Science Letters*, **300**, 1–10, https://doi.org/10.1016/j.epsl.2010.10.005

Freed, A.M., Hirth, G. and Behn, M.D. 2012. Using short-term postseismic displacements to infer the ambient deformation conditions of the upper mantle. *Journal of Geophysical Research: Solid Earth*, **117**, B01409, https://doi.org/10.1029/2011JB008562

Fretwell, P., Pritchard, H.D. *et al*. 2013. Bedmap2: improved ice bed, surface and thickness datasets for Antarctica. *The Cryosphere*, **7**, 375–393, https://doi.org/10.5194/tc-7-375-2013

Fullea, J., Lebedev, S., Martinec, Z. and Celli, N.L. 2021. WINTERC-G: mapping the upper mantle thermochemical heterogeneity from coupled geophysical–petrological inversion of seismic waveforms, heat flow, surface elevation and gravity satellite data. *Geophysical Journal International*, **226**, 146–191, https://doi.org/10.1093/gji/ggab094

Galeotti, S., DeConto, R. *et al*. 2016. Antarctic Ice Sheet variability across the Eocene–Oligocene boundary climate transition. *Science*, **352**, 76–80, https://doi.org/10.1126/science.aab0669

Garbe, J., Albrecht, T., Levermann, A., Donges, J.F. and Winkelmann, R. 2020. The hysteresis of the Antarctic Ice Sheet. *Nature*, **585**, 538–544, https://doi.org/10.1038/s41586-020-2727-5

Geruo, A., Wahr, J. and Zhong, S. 2013. Computations of the viscoelastic response of a 3-D compressible Earth to surface loading: an application to Glacial Isostatic Adjustment in Antarctica and Canada. *Geophysical Journal International*, **192**, 557–572, https://doi.org/10.1093/gji/ggs030

Goelzer, H., Coulon, V., Pattyn, F., de Boer, B. and van de Wal, R. 2020. Brief communication: On calculating the sea-level contribution in marine ice-sheet models. *The Cryosphere*, **14**, 833–840, https://doi.org/10.5194/tc-14-833-2020

Goes, S. and van der Lee, S. 2002. Thermal structure of the North American uppermost mantle inferred from seismic tomography. *Journal of Geophysical Research: Solid Earth*, **107**, ETG 2-1–ETG 2-13, https://doi.org/10.1029/2000JB000049

Golledge, N.R., Fogwill, C.J., Mackintosh, A.N. and Buckley, K.M. 2012. Dynamics of the last glacial maximum Antarctic ice-sheet and its response to ocean forcing. *Proceedings of the National Academy of Sciences of the United States of America*, **109**, 16 052–16 056, https://doi.org/10.1073/pnas.1205385109

Golledge, N.R., Levy, R.H. *et al*. 2013. Glaciology and geological signature of the Last Glacial Maximum Antarctic ice sheet. *Quaternary Science Reviews*, **78**, 225–247, https://doi.org/10.1016/j.quascirev.2013.08.011

Golledge, N.R., Menviel, L., Carter, L., Fogwill, C.J., England, M.H., Cortese, G. and Levy, R.H. 2014. Antarctic contribution to meltwater pulse 1A from reduced Southern Ocean overturning. *Nature Communications*, **5**, 5107, https://doi.org/10.1038/ncomms6107

Gomez, N., Mitrovica, J.X., Huybers, P. and Clark, P.U. 2010. Sea level as a stabilizing factor for marine-ice-sheet grounding lines. *Nature Geoscience*, **3**, 850–853, https://doi.org/10.1038/ngeo1012

Gomez, N., Pollard, D., Mitrovica, J.X., Huybers, P. and Clark, P.U. 2012. Evolution of a coupled marine ice sheet–sea level model. *Journal of Geophysical Research: Earth Surface*, **117**, F01013, https://doi.org/10.1029/2011JF002128

Gomez, N., Pollard, D. and Mitrovica, J.X. 2013. A 3-D coupled ice sheet – sea level model applied to Antarctica through the last

40 ky. *Earth and Planetary Science Letters*, **384**, 88–99, https://doi.org/10.1016/j.epsl.2013.09.042

Gomez, N., Pollard, D. and Holland, D. 2015. Sea-level feedback lowers projections of future Antarctic Ice-Sheet mass loss. *Nature Communications*, **6**, 8798, https://doi.org/10.1038/ncomms9798

Gomez, N., Latychev, K. and Pollard, D. 2018. A coupled ice sheet–sea level model incorporating 3D Earth structure: Variations in Antarctica during the last deglacial retreat. *Journal of Climate*, **31**, 4041–4054, https://doi.org/10.1175/jcli-d-17-0352.1

Gomez, N., Weber, M.E., Clark, P.U., Mitrovica, J.X. and Han, H.K. 2020. Antarctic ice dynamics amplified by Northern Hemisphere sea-level forcing. *Nature*, **587**, 600–604, https://doi.org/10.1038/s41586-020-2916-2

Gowan, E.J., Zhang, X. *et al*. 2021. A new global ice sheet reconstruction for the past 80 000 years. *Nature Communications*, **12**, 1199, https://doi.org/10.1038/s41467-021-21469-w

Greene, C.A., Gwyther, D.E. and Blankenship, D.D. 2017. Antarctic Mapping Tools for Matlab. *Computers & Geosciences*, **104**, 151–157, https://doi.org/10.1016/j.cageo.2016.08.003

Groh, A., Ewert, H. *et al*. 2012. An investigation of Glacial Isostatic Adjustment over the Amundsen Sea sector, West Antarctica. *Global and Planetary Change*, **98-99**, 45–53, https://doi.org/10.1016/j.gloplacha.2012.08.001

Han, H.K., Gomez, N. and Wan, J.X.W. 2022. Capturing the interactions between ice sheets, sea level and the solid Earth on a range of timescales: a new 'time window' algorithm. *Geoscientific Model Development*, **15**, 1355–1373, https://doi.org/10.5194/gmd-15-1355-2022

Handler, M.R., Wysoczanski, R.J. and Gamble, J.A. 2021. Marie Byrd Land lithospheric mantle: a review of the xenolith record. *Geological Society, London, Memoirs*, **56**, https://doi.org/10.1144/M56-2020-17

Hansen, S.E., Graw, J.H. *et al*. 2014. Imaging the Antarctic mantle using adaptively parameterized P-wave tomography: Evidence for heterogeneous structure beneath West Antarctica. *Earth and Planetary Science Letters*, **408**, 66–78, https://doi.org/10.1016/j.epsl.2014.09.043

Hartmann, R., Ebbing, J. and Conrad, C.P. 2020. A Multiple 1D Earth Approach (M1DEA) to account for lateral viscosity variations in solutions of the sea level equation: An application for glacial isostatic adjustment by Antarctic deglaciation. *Journal of Geodynamics*, **135**, 101695, https://doi.org/10.1016/j.jog.2020.101695

Haskell, N. 1935. The motion of a viscous fluid under a surface load. *Physics*, **6**, 265–269, https://doi.org/10.1063/1.1745329

Hattori, A., Aoyama, Y., Okuno, J. and Doi, K. 2021. GNSS observations of GIA-induced crustal deformation in Lützow-Holm Bay, East Antarctica. *Geophysical Research Letters*, **48**, e2021GL093479, https://doi.org/10.1029/2021GL093479

Hay, C.C., Lau, H.C.P. *et al*. 2017. Sea level fingerprints in a region of complex Earth structure: The case of WAIS. *Journal of Climate*, **30**, 1881–1892, https://doi.org/10.1175/jcli-d-16-0388.1

Hayes, G.P. 2017. The finite, kinematic rupture properties of great-sized earthquakes since 1990. *Earth and Planetary Science Letters*, **468**, 94–100, https://doi.org/10.1016/j.epsl.2017.04.003

Henry, C., Das, S. and Woodhouse, J.H. 2000. The great March 25, 1998, Antarctic Plate earthquake: Moment tensor and rupture history. *Journal of Geophysical Research: Solid Earth*, **105**, 16 097–16 118, https://doi.org/10.1029/2000JB900077

Hermans, T.H.J., van der Wal, W. and Broerse, T. 2018. Reversal of the direction of horizontal velocities induced by GIA as a function of mantle viscosity. *Geophysical Research Letters*, **45**, 9597–9604, https://doi.org/10.1029/2018GL078533

Hirth, G. and Kohlstedt, D. 2004. Rheology of the upper mantle and the mantle wedge: A view from the experimentalists. *American Geophysical Union Geophysical Monograph Series*, **138**, 83–105, https://doi.org/10.1029/138GM06

Hodgson, D.A., Whitehouse, P.L. *et al*. 2016. Rapid early Holocene sea-level rise in Prydz Bay, East Antarctica. *Global and Planetary Change*, **139**, 128–140, https://doi.org/10.1016/j.gloplacha.2015.12.020

Hollin, J.T. 1962. On the glacial history of Antarctica. *Journal of Glaciology*, **4**, 173–195, https://doi.org/10.3189/S0022143000027386

Hu, Y. and Wang, K. 2012. Spherical-Earth finite element model of short-term postseismic deformation following the 2004 Sumatra earthquake. *Journal of Geophysical Research: Solid Earth*, **117**, B05404, https://doi.org/10.1029/2012JB009153

Hu, Y., Wang, K., He, J., Klotz, J. and Khazaradze, G. 2004. Three-dimensional viscoelastic finite element model for postseismic deformation of the great 1960 Chile earthquake. *Journal of Geophysical Research: Solid Earth*, **109**, B12403, https://doi.org/10.1029/2004JB003163

Hughes, T.J. 1981. The last great ice sheets: A global view. *In*: Denton, G.H. and Hughes, T.J. (eds) *The Last Great Ice Sheets*. Wiley, New York, 263–317.

Huybrechts, P. 1990. The Antarctic ice sheet during the last glacial–interglacial cycle: a three-dimensional experiment. *Annals of Glaciology*, **14**, 115–119, https://doi.org/10.3189/S0260305500008387

Huybrechts, P. 2002. Sea-level changes at the LGM from ice-dynamic reconstructions of the Greenland and Antarctic ice sheets during the glacial cycles. *Quaternary Science Reviews*, **21**, 203–231, https://doi.org/10.1016/S0277-3791(01)00082-8

Ishiwa, T., Okuno, J.I. and Suganuma, Y. 2021. Excess ice loads in the Indian Ocean sector of East Antarctica during the last glacial period. *Geology*, **49**, 1182–1186, https://doi.org/10.1130/g48830.1

Ivins, E.R. and James, T.S. 2005. Antarctic glacial isostatic adjustment: a new assessment. *Antarctic Science*, **17**, 541–553, https://doi.org/10.1017/S0954102005002968

Ivins, E.R., Raymond, C.A. and James, T.S. 2000. The influence of 5000 year-old and younger glacial mass variability on present-day crustal rebound in the Antarctic Peninsula. *Earth, Planets and Space*, **52**, 1023–1029, https://doi.org/10.1186/BF03352325

Ivins, E.R., James, T.S. and Klemann, V. 2003. Glacial isostatic stress shadowing by the Antarctic ice sheet. *Journal of Geophysical Research: Solid Earth*, **108**, 2560, https://doi.org/10.1029/2002JB002182

Ivins, E.R., Watkins, M.M., Yuan, D.-N., Dietrich, R., Casassa, G. and Rülke, A. 2011. On-land ice loss and glacial isostatic adjustment at the Drake Passage: 2003–2009. *Journal of Geophysical Research: Solid Earth*, **116**, B02403, https://doi.org/10.1029/2010JB007607

Ivins, E.R., James, T.S., Wahr, J.O., Schrama, E.J., Landerer, F.W. and Simon, K.M. 2013. Antarctic contribution to sea level rise observed by GRACE with improved GIA correction. *Journal of Geophysical Research: Solid Earth*, **118**, 3126–3141, https://doi.org/10.1002/jgrb.50208

Ivins, E.R., Caron, L., Adhikari, S., Larour, E. and Scheinert, M. 2020. A linear viscoelasticity for decadal to centennial time scale mantle deformation. *Reports on Progress in Physics*, **83**, 106801, https://doi.org/10.1088/1361-6633/aba346

Ivins, E.R., van der Wal, W., Wiens, D.A., Lloyd, A.J. and Caron, L. 2021. Antarctic upper mantle rheology. *Geological Society, London, Memoirs*, **56**, https://doi.org/10.1144/M56-2020-19

James, T.S. and Ivins, E.R. 1998. Predictions of Antarctic crustal motions driven by present-day ice sheet evolution and by isostatic memory of the Last Glacial Maximum. *Journal of Geophysical Research: Solid Earth*, **103**, 4993–5017, https://doi.org/10.1029/97JB03539

Jamieson, S.S.R., Sugden, D.E. and Hulton, N.R.J. 2010. The evolution of the subglacial landscape of Antarctica. *Earth and Planetary Science Letters*, **293**, 1–27, https://doi.org/10.1016/j.epsl.2010.02.012

Jamieson, T.F. 1865. On the history of the last geological changes in Scotland. *Quarterly Journal of the Geological Society, London*, **21**, 161–204, https://doi.org/10.1144/gsl.Jgs.1865.021.01-02.24

Ji, C., Wald, D.J. and Helmberger, D.V. 2002. Source description of the 1999 Hector Mine, California, earthquake, part I: Wavelet domain inversion theory and resolution analysis. *Bulletin of*

the Seismological Society of America, **92**, 1192–1207, https://doi.org/10.1785/0120000916

Johnson, J.S., Roberts, S.J. *et al*. 2020. Deglaciation of Pope Glacier implies widespread early Holocene ice sheet thinning in the Amundsen Sea sector of Antarctica. *Earth and Planetary Science Letters*, **548**, 116501, https://doi.org/10.1016/j.epsl.2020.116501

Johnston, A.C. 1987. Suppression of earthquakes by large continental ice sheets. *Nature*, **330**, 467–469, https://doi.org/10.1038/330467a0

Johnston, P. 1993. The effect of spatially non-uniform water loads on prediction of sea-level change. *Geophysical Journal International*, **114**, 615–634, https://doi.org/10.1111/j.1365-246X.1993.tb06992.x

Jones, R.S., Whitehouse, P.L., Bentley, M.J., Small, D. and Dalton, A.S. 2019. Impact of glacial isostatic adjustment on cosmogenic surface-exposure dating. *Quaternary Science Reviews*, **212**, 206–212, https://doi.org/10.1016/j.quascirev.2019.03.012

Kachuck, S.B., Martin, D.F., Bassis, J.N. and Price, S.F. 2020. Rapid viscoelastic deformation slows marine ice sheet instability at Pine Island Glacier. *Geophysical Research Letters*, **47**, e2019GL086446, https://doi.org/10.1029/2019GL086446

Kalberg, T., Gohl, K., Eagles, G. and Spiegel, C. 2015. Rift processes and crustal structure of the Amundsen Sea Embayment, West Antarctica, from 3D potential field modelling. *Marine Geophysical Research*, **36**, 263–279, https://doi.org/10.1007/s11001-015-9261-0

Kaufmann, G. and Lambeck, K. 2002. Glacial isostatic adjustment and the radial viscosity profile from inverse modeling. *Journal of Geophysical Research: Solid Earth*, **107**, ETG 5-1–ETG 5-15, https://doi.org/10.1029/2001JB000941

Kaufmann, G., Wu, P. and Ivins, E.R. 2005. Lateral viscosity variations beneath Antarctica and their implications on regional rebound motions and seismotectonics. *Journal of Geodynamics*, **39**, 165–181, https://doi.org/10.1016/j.jog.2004.08.009

Kawamata, M., Suganuma, Y., Doi, K., Misawa, K., Hirabayashi, M., Hattori, A. and Sawagaki, T. 2020. Abrupt Holocene ice-sheet thinning along the southern Soya Coast, Lützow-Holm Bay, East Antarctica, revealed by glacial geomorphology and surface exposure dating. *Quaternary Science Reviews*, **247**, 106540, https://doi.org/10.1016/j.quascirev.2020.106540

Khazaradze, G. and Klotz, J. 2003. Short- and long-term effects of GPS measured crustal deformation rates along the south central Andes. *Journal of Geophysical Research: Solid Earth*, **108**, 2289, https://doi.org/10.1029/2002JB001879

Khazaradze, G., Wang, K., Klotz, J., Hu, Y. and He, J. 2002. Prolonged post-seismic deformation of the 1960 great Chile earthquake and implications for mantle rheology. *Geophysical Research Letters*, **29**, 7-1–7-4, https://doi.org/10.1029/2002GL015986

King, M.A. 2013. Progress in modelling and observing Antarctic glacial isostatic adjustment. *Astronomy & Geophysics*, **54**, 4.33–34.38, https://doi.org/10.1093/astrogeo/att122

King, M.A. and Santamaría-Gómez, A. 2016. Ongoing deformation of Antarctica following recent Great Earthquakes. *Geophysical Research Letters*, **43**, 1918–1927, https://doi.org/10.1002/2016GL067773

King, M.A., Whitehouse, P.L. and van der Wal, W. 2016. Incomplete separability of Antarctic plate rotation from glacial isostatic adjustment deformation within geodetic observations. *Geophysical Journal International*, **204**, 324–330, https://doi.org/10.1093/gji/ggv461

Kingslake, J., Scherer, R.P. *et al*. 2018. Extensive retreat and re-advance of the West Antarctic Ice Sheet during the Holocene. *Nature*, **558**, 430–434, https://doi.org/10.1038/s41586-018-0208-x

Konfal, S.A., Wilson, T.J. *et al*. 2013. Palaeoshoreline records of glacial isostatic adjustment in the Dry Valleys region, Antarctica. *Geological Society, London, Special Publications*, **381**, 455–467, https://doi.org/10.1144/SP381.26

Konfal, S.A., Wilson, T.J. *et al*. 2018. Utilizing GPS to investigate past ice mass change in the Ross Sea region, Antarctica. Abstract #G43B-0716 presented at the 2018 AGU Fall Meeting, 10–14 December 2018, Washington, DC.

Konrad, H., Thoma, M., Sasgen, I., Klemann, V., Grosfeld, K., Barbi, D. and Martinec, Z. 2014. The deformational response of a viscoelastic solid Earth model coupled to a thermomechanical ice sheet model. *Surveys in Geophysics*, **35**, 1441–1458, https://doi.org/10.1007/s10712-013-9257-8

Konrad, H., Sasgen, I., Pollard, D. and Klemann, V. 2015. Potential of the solid-Earth response for limiting long-term West Antarctic Ice Sheet retreat in a warming climate. *Earth and Planetary Science Letters*, **432**, 254–264, https://doi.org/10.1016/j.epsl.2015.10.008

Lambeck, K., Yokoyama, Y., Johnston, P. and Purcell, A. 2000. Global ice volumes at the Last Glacial Maximum and early Lateglacial. *Earth and Planetary Science Letters*, **181**, 513–527, https://doi.org/10.1016/S0012-821X(00)00223-5

Lambeck, K., Rouby, H., Purcell, A., Sun, Y. and Sambridge, M. 2014. Sea level and global ice volumes from the Last Glacial Maximum to the Holocene. *Proceedings of the National Academy of Sciences of the United States of America*, **111**, 15 296–15 303, https://doi.org/10.1073/pnas.1411762111

Lambeck, K., Purcell, A. and Zhao, S. 2017. The North American Late Wisconsin ice sheet and mantle viscosity from glacial rebound analyses. *Quaternary Science Reviews*, **158**, 172–210, https://doi.org/10.1016/j.quascirev.2016.11.033

Larour, E., Seroussi, H., Adhikari, S., Ivins, E., Caron, L., Morlighem, M. and Schlegel, N. 2019. Slowdown in Antarctic mass loss from solid Earth and sea-level feedbacks. *Science*, **364**, eaav7908, https://doi.org/10.1126/science.aav7908

Larsen, C.F., Motyka, R.J., Freymueller, J.T., Echelmeyer, K.A. and Ivins, E.R. 2005. Rapid viscoelastic uplift in southeast Alaska caused by post-Little Ice Age glacial retreat. *Earth and Planetary Science Letters*, **237**, 548–560, https://doi.org/10.1016/j.epsl.2005.06.032

Larter, R.D. and Barker, P.F. 1991. Effects of ridge crest–trench interaction on Antarctic–Phoenix Spreading: Forces on a young subducting plate. *Journal of Geophysical Research: Solid Earth*, **96**, 19 583–19 607, https://doi.org/10.1029/91JB02053

Latychev, K., Mitrovica, J.X., Tromp, J., Tamisiea, M.E., Komatitsch, D. and Christara, C.C. 2005. Glacial isostatic adjustment on 3-D Earth models: a finite-volume formulation. *Geophysical Journal International*, **161**, 421–444, https://doi.org/10.1111/j.1365-246X.2005.02536.x

Lau, H.C.P., Mitrovica, J.X., Austermann, J., Crawford, O., Al-Attar, D. and Latychev, K. 2016. Inferences of mantle viscosity based on ice age data sets: Radial structure. *Journal of Geophysical Research: Solid Earth*, **121**, 6991–7012, https://doi.org/10.1002/2016JB013043

Lau, H.C.P., Austermann, J., Holtzman, B.K., Havlin, C., Lloyd, A.J., Book, C. and Hopper, E. 2021. Frequency dependent mantle viscoelasticity via the complex viscosity: Cases from Antarctica. *Journal of Geophysical Research: Solid Earth*, **126**, e2021JB022622, https://doi.org/10.1029/2021JB022622

Lawver, L.A., Sloan, B.J. *et al*. 1996. Distributed, active extension in Bransfield basin Antarctic Peninsula: Evidence from multibeam bathymetry. *GSA Today*, **6**, 1–6.

Lear, C.H., Elderfield, H. and Wilson, P.A. 2000. Cenozoic deep-sea temperatures and global ice volumes from Mg/Ca in benthic foraminiferal calcite. *Science*, **287**, 269–272, https://doi.org/10.1126/science.287.5451.269

Le Meur, E. and Huybrechts, P. 1996. A comparison of different ways of dealing with isostasy: examples from modelling the Antarctic ice sheet during the last glacial cycle. *Annals of Glaciology*, **23**, 309–317, https://doi.org/10.3189/S0260305500013586

Lloyd, A.J., Wiens, D.A. *et al*. 2020. Seismic structure of the Antarctic upper mantle imaged with adjoint tomography. *Journal of Geophysical Research: Solid Earth*, **125**, https://doi.org/10.1029/2019JB017823

Lohman, R.B. and Simons, M. 2005. Some thoughts on the use of InSAR data to constrain models of surface deformation: Noise structure and data downsampling. *Geochemistry,*

Geophysics, Geosystems, **6**, Q01007, https://doi.org/10.1029/2004GC000841

Lough, A.C., Wiens, D.A. and Nyblade, A. 2018. Reactivation of ancient Antarctic rift zones by intraplate seismicity. *Nature Geoscience*, **11**, 515–519, https://doi.org/10.1038/s41561-018-0140-6

Lucas, E.M., Nyblade, A.A. *et al*. 2021. Seismicity and Pn velocity structure of central West Antarctica. *Geochemistry, Geophysics, Geosystems*, **22**, e2020GC009471, https://doi.org/10.1029/2020GC009471

Mackintosh, A., Golledge, N. *et al*. 2011. Retreat of the East Antarctic ice sheet during the last glacial termination. *Nature Geoscience*, **4**, 195–202, https://doi.org/10.1038/ngeo1061

Mackintosh, A.N., Verleyen, E. *et al*. 2014. Retreat history of the East Antarctic Ice Sheet since the Last Glacial Maximum. *Quaternary Science Reviews*, **100**, 10–30, https://doi.org/10.1016/j.quascirev.2013.07.024

Maris, M.N.A., de Boer, B., Ligtenberg, S.R.M., Crucifix, M., van de Berg, W.J. and Oerlemans, J. 2014. Modelling the evolution of the Antarctic ice sheet since the last interglacial. *The Cryosphere*, **8**, 1347–1360, https://doi.org/10.5194/tc-8-1347-2014

Maris, M.N.A., van Wessem, J.M., van de Berg, W.J., de Boer, B. and Oerlemans, J. 2015. A model study of the effect of climate and sea-level change on the evolution of the Antarctic Ice Sheet from the Last Glacial Maximum to 2100. *Climate Dynamics*, **45**, 837–851, https://doi.org/10.1007/s00382-014-2317-z

Martin, A.P. 2021. A review of the composition and chemistry of peridotite mantle xenoliths in volcanic rocks from Antarctica and their relevance to petrological and geophysical models for the lithospheric mantle. *Geological Society, London, Memoirs*, **56**, https://doi.org/10.1144/M56-2021-26

Martin, A.P., Cooper, A.F. and Price, R.C. 2014. Increased mantle heat flow with on-going rifting of the West Antarctic rift system inferred from characterisation of plagioclase peridotite in the shallow Antarctic mantle. *Lithos*, **190–191**, 173–190, https://doi.org/10.1016/j.lithos.2013.12.012

Martin, A.P., van der Wal, W. and de Boer, B. 2022. An introduction to the geochemistry and geophysics of the Antarctic mantle. *Geological Society, London, Memoirs*, **56**, https://doi.org/10.1144/M56-2022-21

Martinec, Z. 2000. Spectral–finite element approach to three-dimensional viscoelastic relaxation in a spherical earth. *Geophysical Journal International*, **142**, 117–141, https://doi.org/10.1046/j.1365-246x.2000.00138.x

Martín-Español, A., King, M.A., Zammit-Mangion, A., Andrews, S.B., Moore, P. and Bamber, J.L. 2016*a*. An assessment of forward and inverse GIA solutions for Antarctica. *Journal of Geophysical Research: Solid Earth*, **121**, 6947–6965, https://doi.org/10.1002/2016JB013154

Martín-Español, A., Zammit-Mangion, A. *et al*. 2016*b*. Spatial and temporal Antarctic Ice Sheet mass trends, glacio-isostatic adjustment, and surface processes from a joint inversion of satellite altimeter, gravity, and GPS data. *Journal of Geophysical Research: Earth Surface*, **121**, 182–200, https://doi.org/10.1002/2015JF003550

Miller, K.G., Wright, J.D. and Fairbanks, R.G. 1991. Unlocking the Ice House: Oligocene–Miocene oxygen isotopes, eustasy, and margin erosion. *Journal of Geophysical Research: Solid Earth*, **96**, 6829–6848, https://doi.org/10.1029/90JB02015

Milne, G.A. and Mitrovica, J.X. 1998. Postglacial sea-level change on a rotating Earth. *Geophysical Journal International*, **133**, 1–19, https://doi.org/10.1046/j.1365-246X.1998.1331455.x

Milne, G.A., Mitrovica, J.X. and Davis, J.L. 1999. Near-field hydro-isostasy: the implementation of a revised sea-level equation. *Geophysical Journal International*, **139**, 464–482, https://doi.org/10.1046/j.1365-246x.1999.00971.x

Mitrovica, J.X. 1996. Haskell [1935] revisited. *Journal of Geophysical Research: Solid Earth*, **101**, 555–569, https://doi.org/10.1029/95JB03208

Mitrovica, J.X. and Peltier, W.R. 1991. On postglacial geoid subsidence over the equatorial oceans. *Journal of Geophysical Research: Solid Earth*, **96**, 20053–20071, https://doi.org/10.1029/91JB01284

Mitrovica, J.X. and Milne, G.A. 2002. On the origin of late Holocene sea-level highstands within equatorial ocean basins. *Quaternary Science Reviews*, **21**, 2179–2190, https://doi.org/10.1016/S0277-3791(02)00080-X

Mitrovica, J.X., Gomez, N. and Clark, P.U. 2009. The sea-level fingerprint of West Antarctic collapse. *Science*, **323**, 753–753, https://doi.org/10.1126/science.1166510

Morelli, A. and Danesi, S. 2004. Seismological imaging of the Antarctic continental lithosphere: a review. *Global and Planetary Change*, **42**, 155–165, https://doi.org/10.1016/j.gloplacha.2003.12.005

Morlighem, M., Rignot, E. *et al*. 2020. Deep glacial troughs and stabilizing ridges unveiled beneath the margins of the Antarctic ice sheet. *Nature Geoscience*, **13**, 132–137, https://doi.org/10.1038/s41561-019-0510-8

Naish, T.R., Duncan, B. *et al*. 2022. Antarctic Ice Sheet dynamics during the Late Oligocene and Early Miocene: climatic conundrums revisited. *In*: Florindo, F., Siegert, M., Santis, L.D. and Naish, T. (eds) *Antarctic Climate Evolution*. 2nd edn. Elsevier, Amsterdam, 363–387, https://doi.org/10.1016/B978-0-12-819109-5.00013-X

Nakada, M. 1983. Rheological structure of the earth's mantle derived from glacial rebound in Laurentide. *Journal of Physics of the Earth*, **31**, 349–386, https://doi.org/10.4294/jpe1952.31.349

Nakada, M., Kimura, R., Okuno, J., Moriwaki, K., Miura, H. and Maemoku, H. 2000. Late Pleistocene and Holocene melting history of the Antarctic ice sheet derived from sea-level variations. *Marine Geology*, **167**, 85–103, https://doi.org/10.1016/S0025-3227(00)00018-9

Nakiboglu, S.M., Lambeck, K. and Aharon, P. 1983. Postglacial sea-levels in the Pacific: Implications with respect to deglaciation regime and local tectonics. *Tectonophysics*, **91**, 335–358, https://doi.org/10.1016/0040-1951(83)90049-5

Nettles, M., Wallace, T.C. and Beck, S.L. 1999. The March 25, 1998 Antarctic Plate Earthquake. *Geophysical Research Letters*, **26**, 2097–2100, https://doi.org/10.1029/1999GL900387

Nield, G.A., Barletta, V.R. *et al*. 2014. Rapid bedrock uplift in the Antarctic Peninsula explained by viscoelastic response to recent ice unloading. *Earth and Planetary Science Letters*, **397**, 32–41, https://doi.org/10.1016/j.epsl.2014.04.019

Nield, G.A., Whitehouse, P.L., van der Wal, W., Blank, B., O'Donnell, J.P. and Stuart, G.W. 2018. The impact of lateral variations in lithospheric thickness on glacial isostatic adjustment in West Antarctica. *Geophysical Journal International*, **214**, 811–824, https://doi.org/10.1093/gji/ggy158

Nield, G.A., King, M.A., Steffen, R. and Blank, B. 2022. A global, spherical finite-element model for post-seismic deformation using Abaqus. *Geoscientific Model Development*, **15**, 2489–2503, https://doi.org/10.5194/gmd-15-2489-2022

O'Donnell, J.P., Selway, K. *et al*. 2017. The uppermost mantle seismic velocity and viscosity structure of central West Antarctica. *Earth and Planetary Science Letters*, **472**, 38–49, https://doi.org/10.1016/j.epsl.2017.05.016

Oerlemans, J. 1980. Model experiments on the 100,000-yr glacial cycle. *Nature*, **287**, 430–432, https://doi.org/10.1038/287430a0

Okuno, J.I. and Miura, H. 2013. Last deglacial relative sea level variations in Antarctica derived from glacial isostatic adjustment modelling. *Geoscience Frontiers*, **4**, 623–632, https://doi.org/10.1016/j.gsf.2012.11.004

Oude Egbrink, D. 2017. *Modelling the Last Glacial Ice Sheet on Antarctica with Laterally Varying Relaxation Time*. MSc dissertation, Delft University of Technology, Delft, The Netherlands.

Pan, L., Powell, E.M. *et al*. 2021. Rapid postglacial rebound amplifies global sea level rise following West Antarctic Ice Sheet collapse. *Science Advances*, **7**, eabf7787, https://doi.org/10.1126/sciadv.abf7787

Panter, K.S. and Martin, A.P. 2021. West Antarctic mantle deduced from mafic magmatism. *Geological Society, London, Memoirs*, **56**, https://doi.org/10.1144/M56-2021-10

Panter, K.S., Castillo, P. *et al*. 2018. Melt origin across a rifted continental margin: A case for subduction-related metasomatic agents in the lithospheric source of alkaline basalt, NW Ross

Sea, Antarctica. *Journal of Petrology*, **59**, 517–558, https://doi.org/10.1093/petrology/egy036

Pappa, F. and Ebbing, J. 2021. Gravity, magnetics and geothermal heat flow of the Antarctic lithospheric crust and mantle. *Geological Society, London, Memoirs*, **56**, https://doi.org/10.1144/M56-2020-5

Pappa, F., Ebbing, J., Ferraccioli, F. and van der Wal, W. 2019. Modeling satellite gravity gradient data to derive density, temperature, and viscosity structure of the Antarctic lithosphere. *Journal of Geophysical Research: Solid Earth*, **124**, 12 053–12 076, https://doi.org/10.1029/2019JB017997

Parizek, B.R. and Alley, R.B. 2004. Ice thickness and isostatic imbalances in the Ross Embayment, West Antarctica: model results. *Global and Planetary Change*, **42**, 265–278, https://doi.org/10.1016/j.gloplacha.2003.09.005

Parrenin, F., Dreyfus, G. *et al*. 2007. 1-D-ice flow modelling at EPICA Dome C and Dome Fuji, East Antarctica. *Climate of the Past*, **3**, 243–259, https://doi.org/10.5194/cp-3-243-2007

Pattyn, F., Favier, L., Sun, S. and Durand, G. 2017. Progress in numerical modeling of Antarctic ice-sheet dynamics. *Current Climate Change Reports*, **3**, 174–184, https://doi.org/10.1007/s40641-017-0069-7

Paulson, A., Zhong, S. and Wahr, J. 2005. Modelling post-glacial rebound with lateral viscosity variations. *Geophysical Journal International*, **163**, 357–371, https://doi.org/10.1111/j.1365-246X.2005.02645.x

Paulson, A., Zhong, S. and Wahr, J. 2007. Limitations on the inversion for mantle viscosity from postglacial rebound. *Geophysical Journal International*, **168**, 1195–1209, https://doi.org/10.1111/j.1365-246X.2006.03222.x

Paxman, G.J.G. 2021. Antarctic palaeotopography. *Geological Society, London, Memoirs*, **56**, https://doi.org/10.1144/M56-2020-7

Paxman, G.J.G., Jamieson, S.S.R., Hochmuth, K., Gohl, K., Bentley, M.J., Leitchenkov, G. and Ferraccioli, F. 2019. Reconstructions of Antarctic topography since the Eocene–Oligocene boundary. *Palaeogeography, Palaeoclimatology, Palaeoecology*, **535**, 109346, https://doi.org/10.1016/j.palaeo.2019.109346

Peltier, W.R. 1974. The impulse response of a Maxwell Earth. *Reviews of Geophysics*, **12**, 649–669, https://doi.org/10.1029/RG012i004p00649

Peltier, W.R. 1976. Glacial-isostatic adjustment – II. The inverse problem. *Geophysical Journal International*, **46**, 669–705, https://doi.org/10.1111/j.1365-246X.1976.tb01253.x

Peltier, W.R. 1988. Lithospheric thickness, Antarctic deglaciation history, and ocean basin discretization effects in a global model of postglacial sea level change: A summary of some sources of nonuniqueness. *Quaternary Research*, **29**, 93–112, https://doi.org/10.1016/0033-5894(88)90054-3

Peltier, W.R. 1994. Ice Age paleotopography. *Science*, **265**, 195–201, https://doi.org/10.1126/science.265.5169.195

Peltier, W.R. 2004. Global glacial isostasy and the surface of the ice-age earth: the ICE-5G (VM2) model and GRACE. *Annual Review of Earth and Planetary Sciences*, **32**, 111–149, https://doi.org/10.1146/annurev.earth.32.082503.144359

Pollard, D., Chang, W., Haran, M., Applegate, P. and DeConto, R. 2016. Large ensemble modeling of the last deglacial retreat of the West Antarctic Ice Sheet: comparison of simple and advanced statistical techniques. *Geoscientific Model Development*, **9**, 1697–1723, https://doi.org/10.5194/gmd-9-1697-2016

Pollard, D., Gomez, N. and Deconto, R.M. 2017. Variations of the Antarctic Ice Sheet in a coupled ice sheet–Earth–sea level model: Sensitivity to viscoelastic Earth properties. *Journal of Geophysical Research: Earth Surface*, **122**, 2124–2138, https://doi.org/10.1002/2017JF004371

Pollitz, F.F. 1997. Gravitational viscoelastic postseismic relaxation on a layered spherical Earth. *Journal of Geophysical Research: Solid Earth*, **102**, 17 921–17 941, https://doi.org/10.1029/97JB01277

Pollitz, F.F. 2005. Transient rheology of the upper mantle beneath central Alaska inferred from the crustal velocity field following the 2002 Denali earthquake. *Journal of Geophysical Research B: Solid Earth*, **110**, 1–16, https://doi.org/10.1029/2005JB003672

Pollitz, F.F. and Thatcher, W. 2010. On the resolution of shallow mantle viscosity structure using postearthquake relaxation data: Application to the 1999 Hector Mine, California, earthquake. *Journal of Geophysical Research: Solid Earth*, **115**, B10412, https://doi.org/10.1029/2010JB007405

Powell, E., Gomez, N., Hay, C., Latychev, K. and Mitrovica, J.X. 2020. Viscous effects in the solid Earth response to modern Antarctic ice mass flux: Implications for geodetic studies of WAIS stability in a warming world. *Journal of Climate*, **33**, 443–459, https://doi.org/10.1175/jcli-d-19-0479.1

Powell, E.M., Pan, L., Hoggard, M.J., Latychev, K., Gomez, N., Austermann, J. and Mitrovica, J.X. 2021. The impact of 3-D Earth structure on far-field sea level following interglacial West Antarctic Ice Sheet collapse. *Quaternary Science Reviews*, **273**, 107256, https://doi.org/10.1016/j.quascirev.2021.107256

Quiquet, A., Dumas, C., Ritz, C., Peyaud, V. and Roche, D.M. 2018. The GRISLI ice sheet model (version 2.0): calibration and validation for multi-millennial changes of the Antarctic ice sheet. *Geoscientific Model Development*, **11**, 5003–5025, https://doi.org/10.5194/gmd-11-5003-2018

Ranalli, G. 1995. *Rheology of the Earth*. Springer, Dordrecht, The Netherlands.

Reading, A.M. 2007. The seismicity of the Antarctic plate. *Geological Society of America Special Papers*, **425**, 285–298, https://doi.org/10.1130/2007.2425(18)

Rignot, E. 2006. Changes in ice dynamics and mass balance of the Antarctic ice sheet. *Philosophical Transactions of the Royal Society A: Mathematical, Physical and Engineering Sciences*, **364**, 1637–1655, https://doi.org/10.1098/rsta.2006.1793

Riva, R.E.M., Gunter, B.C. *et al*. 2009. Glacial Isostatic Adjustment over Antarctica from combined ICESat and GRACE satellite data. *Earth and Planetary Science Letters*, **288**, 516–523, https://doi.org/10.1016/j.epsl.2009.10.013

Rovere, A., Raymo, M.E., Mitrovica, J.X., Hearty, P.J., O'Leary, M.J. and Inglis, J.D. 2014. The Mid-Pliocene sea-level conundrum: Glacial isostasy, eustasy and dynamic topography. *Earth and Planetary Science Letters*, **387**, 27–33, https://doi.org/10.1016/j.epsl.2013.10.030

Rychert, C.A., Harmon, N., Constable, S. and Wang, S. 2020. The Nature of the Lithosphere-Asthenosphere Boundary. *Journal of Geophysical Research: Solid Earth*, **125**, e2018JB016463, https://doi.org/10.1029/2018JB016463

Sabadini, R., Yuen, D.A. and Gasperini, P. 1985. The effects of transient rheology on the interpretation of lower mantle viscosity. *Geophysical Research Letters*, **12**, 361–364, https://doi.org/10.1029/GL012i006p00361

Sabadini, R., Vermeersen, B. and Cambiotti, G. 2016. *Global Dynamics of the Earth: Applications of Viscoelastic Relaxation Theory to Solid-Earth and Planetary Geophysics*. Springer, Dordrecht, The Netherlands.

Samrat, N.H., King, M.A., Watson, C., Hooper, A., Chen, X., Barletta, V.R. and Bordoni, A. 2020. Reduced ice mass loss and three-dimensional viscoelastic deformation in northern Antarctic Peninsula inferred from GPS. *Geophysical Journal International*, **222**, 1013–1022, https://doi.org/10.1093/gji/ggaa229

Samrat, N.H., King, M.A., Watson, C., Hay, A., Barletta, V.R. and Bordoni, A. 2021. Upper mantle viscosity underneath northern Marguerite Bay, Antarctic Peninsula constrained by bedrock uplift and ice mass variability. *Geophysical Research Letters*, **48**, e2021GL097065, https://doi.org/10.1029/2021GL097065

Scheinert, M., Engels, O., Schrama, E.J.O., van der Wal, W. and Horwath, M. 2021. Geodetic observations for constraining mantle processes in Antarctica. *Geological Society, London, Memoirs*, **56**, https://doi.org/10.1144/M56-2021-22

Schoof, C. 2007. Ice sheet grounding line dynamics: Steady states, stability, and hysteresis. *Journal of Geophysical Research: Earth Surface*, **112**, F03S28, https://doi.org/10.1029/2006JF000664

Schumacher, M., King, M.A., Rougier, J., Sha, Z., Khan, S.A. and Bamber, J.L. 2018. A new global GPS data set for testing and

improving modelled GIA uplift rates. *Geophysical Journal International*, **214**, 2164–2176, https://doi.org/10.1093/gji/ggy235

Shao, Z., Zhan, W., Zhang, L. and Xu, J. 2016. Analysis of the far-field co-seismic and post-seismic responses caused by the 2011 M_W 9.0 Tohoku-Oki earthquake. *Pure and Applied Geophysics*, **173**, 411–424, https://doi.org/10.1007/s00024-015-1131-9

Shepherd, A., Ivins, E. *et al*. 2018. Mass balance of the Antarctic Ice Sheet from 1992 to 2017. *Nature*, **558**, 219–222, https://doi.org/10.1038/s41586-018-0179-y

Siddall, M., Milne, G.A. and Masson-Delmotte, V. 2012. Uncertainties in elevation changes and their impact on Antarctic temperature records since the end of the last glacial period. *Earth and Planetary Science Letters*, **315–316**, 12–23, https://doi.org/10.1016/j.epsl.2011.04.032

Siegert, M. and Golledge, N.R. 2022. Advances in numerical modelling of the Antarctic ice sheet. *In*: Florindo, F., Siegert, M., Santis, L.D. and Naish, T. (eds) *Antarctic Climate Evolution*. 2nd edn. Elsevier, Amsterdam, 199–218, https://doi.org/10.1016/B978-0-12-819109-5.00006-2

Siegert, M., Hein, A.S., White, D.A., Gore, D.B., De Santis, L. and Hillenbrand, C.-D. 2022. Antarctic Ice Sheet changes since the Last Glacial Maximum. *In*: Florindo, F., Siegert, M., Santis, L.D. and Naish, T. (eds) *Antarctic Climate Evolution*. 2nd edn. Elsevier, Amsterdam, 623–687, https://doi.org/10.1016/B978-0-12-819109-5.00002-5

Siegert, M.J., Kingslake, J. *et al*. 2019. Major ice sheet change in the Weddell Sea sector of West Antarctica over the last 5,000 years. *Reviews of Geophysics*, **57**, 1197–1223, https://doi.org/10.1029/2019RG000651

Sigmundsson, F. 1991. Post-glacial rebound and asthenosphere viscosity in Iceland. *Geophysical Research Letters*, **18**, 1131–1134, https://doi.org/10.1029/91GL01342

Simms, A.R., Whitehouse, P.L., Simkins, L.M., Nield, G., DeWitt, R. and Bentley, M.J. 2018. Late Holocene relative sea levels near Palmer Station, northern Antarctic Peninsula, strongly controlled by late Holocene ice-mass changes. *Quaternary Science Reviews*, **199**, 49–59, https://doi.org/10.1016/j.quascirev.2018.09.017

Simms, A.R., Lisiecki, L., Gebbie, G., Whitehouse, P.L. and Clark, J.F. 2019. Balancing the last glacial maximum (LGM) sea-level budget. *Quaternary Science Reviews*, **205**, 143–153, https://doi.org/10.1016/j.quascirev.2018.12.018

Simms, A.R., Bentley, M.J., Simkins, L.M., Zurbuchen, J., Reynolds, L.C., DeWitt, R. and Thomas, E.R. 2021. Evidence for a 'Little Ice Age' glacial advance within the Antarctic Peninsula – Examples from glacially-overrun raised beaches. *Quaternary Science Reviews*, **271**, 107195, https://doi.org/10.1016/j.quascirev.2021.107195

Smellie, J.L. 2018. Glaciovolcanism: A 21st century proxy for palaeo-ice. *In*: Menzies, J. and van der Meer, J.J.M. (eds) *Past Glacial Environments*. 2nd edn. Elsevier, Amsterdam, 335–375, https://doi.org/10.1016/B978-0-08-100524-8.00010-5

Smellie, J.L. 2021. Bransfield Strait and James Ross Island: volcanology. *Geological Society, London, Memoirs*, **55**, 227–284, https://doi.org/10.1144/m55-2018-58

Smellie, J.L., Haywood, A.M., Hillenbrand, C.-D., Lunt, D.J. and Valdes, P.J. 2009. Nature of the Antarctic Peninsula Ice Sheet during the Pliocene: Geological evidence and modelling results compared. *Earth-Science Reviews*, **94**, 79–94, https://doi.org/10.1016/j.earscirev.2009.03.005

Smellie, J.L., Rocchi, S., Gemelli, M., Di Vincenzo, G. and Armienti, P. 2011. A thin predominantly cold-based Late Miocene East Antarctic ice sheet inferred from glaciovolcanic sequences in northern Victoria Land, Antarctica. *Palaeogeography, Palaeoclimatology, Palaeoecology*, **307**, 129–149, https://doi.org/10.1016/j.palaeo.2011.05.008

Smellie, J.L., Panter, K.S. and Geyer, A. 2021. Introduction to volcanism in Antarctica: 200 million years of subduction, rifting and continental break-up. *Geological Society, London, Memoirs*, **55**, 1–6, https://doi.org/10.1144/m55-2020-14

Spiegel, C., Lindow, J. *et al*. 2016. Tectonomorphic evolution of Marie Byrd Land – Implications for Cenozoic rifting activity and onset of West Antarctic glaciation. *Global and Planetary Change*, **145**, 98–115, https://doi.org/10.1016/j.gloplacha.2016.08.013

Steffen, H. and Wu, P. 2011. Glacial isostatic adjustment in Fennoscandia – A review of data and modeling. *Journal of Geodynamics*, **52**, 169–204, https://doi.org/10.1016/j.jog.2011.03.002

Stein, S. and Mazzotti, S. 2007. *Continental Intraplate Earthquakes: Science, Hazard, and Policy Issues*. Geological Society of America Special Papers, **425**, https://doi.org/10.1130/SPE425

Stocchi, P., Escutia, C. *et al*. 2013. Relative sea-level rise around East Antarctica during Oligocene glaciation. *Nature Geoscience*, **6**, 380–384, https://doi.org/10.1038/ngeo1783

Stuhne, G.R. and Peltier, W.R. 2015. Reconciling the ICE-6G_C reconstruction of glacial chronology with ice sheet dynamics: The cases of Greenland and Antarctica. *Journal of Geophysical Research: Earth Surface*, **120**, 1841–1865, https://doi.org/10.1002/2015JF003580

Stuiver, M., Denton, G.H., Hughes, T.J. and Fastook, J.L. 1981. History of the marine ice sheet in West Antarctica during the last glaciation: a working hypothesis. *In*: Denton, G.H. and Hughes, T.J. (eds) *The Last Great Ice Sheets*. Wiley-Interscience, New York, 319–436.

Sun, T., Wang, K. and He, J. 2018. Crustal deformation following great subduction earthquakes controlled by earthquake size and mantle rheology. *Journal of Geophysical Research: Solid Earth*, **123**, 5323–5345, https://doi.org/10.1029/2017JB01 5242

Suess, E. 1888. *Das Antlitz der Erde, Vol. 2, Part 3: Die Meere der Erde.* F. Tempsky, Vienna.

Tarasov, L., Dyke, A.S., Neal, R.M. and Peltier, W.R. 2012. A data-calibrated distribution of deglacial chronologies for the North American ice complex from glaciological modeling. *Earth and Planetary Science Letters*, **315-316**, 30–40, https://doi.org/10.1016/j.epsl.2011.09.010

Thomas, I.D., King, M.A. *et al*. 2011. Widespread low rates of Antarctic glacial isostatic adjustment revealed by GPS observations. *Geophysical Research Letters*, **38**, https://doi.org/10.1029/2011GL049277

Thomas, R.H. 1979. The dynamics of marine ice sheets. *Journal of Glaciology*, **24**, 167–177, https://doi.org/10.3189/S0022143000014726

Tsuboi, S., Kikuchi, M., Yamanaka, Y. and Kanao, M. 2000. The March 25, 1998 Antarctic Earthquake: Great earthquake caused by postglacial rebound. *Earth, Planets and Space*, **52**, 133–136, https://doi.org/10.1186/BF03351621

Turney, C.S.M., Fogwill, C.J. *et al*. 2020. Early Last Interglacial ocean warming drove substantial ice mass loss from Antarctica. *Proceedings of the National Academy of Sciences of the United States of America*, **117**, 3996–4006, https://doi.org/10.1073/pnas.1902469117

van der Wal, W., Kurtenbach, E., Kusche, J. and Vermeersen, B. 2011. Radial and tangential gravity rates from GRACE in areas of glacial isostatic adjustment. *Geophysical Journal International*, **187**, 797–812, https://doi.org/10.1111/j.1365-246X.2011.05206.x

van der Wal, W., Barnhoorn, A., Stocchi, P., Gradmann, S., Wu, P., Drury, M. and Vermeersen, B. 2013. Glacial isostatic adjustment model with composite 3-D Earth rheology for Fennoscandia. *Geophysical Journal International*, **194**, 61–77, https://doi.org/10.1093/gji/ggt099

van der Wal, W., Whitehouse, P.L. and Schrama, E.J.O. 2015. Effect of GIA models with 3D composite mantle viscosity on GRACE mass balance estimates for Antarctica. *Earth and Planetary Science Letters*, **414**, 134–143, https://doi.org/10.1016/j.epsl.2015.01.001

Verleyen, E., Tavernier, I. *et al*. 2017. Ice sheet retreat and glacio-isostatic adjustment in Lützow-Holm Bay, East Antarctica. *Quaternary Science Reviews*, **169**, 85–98, https://doi.org/10.1016/j.quascirev.2017.06.003

Wahr, J., Wingham, D. and Bentley, C. 2000. A method of combining ICESat and GRACE satellite data to constrain Antarctic mass

balance. *Journal of Geophysical Research: Solid Earth*, **105**, 16 279–16 294, https://doi.org/10.1029/2000JB900113

Walcott, R.I. 1972. Late Quaternary vertical movements in eastern North America: Quantitative evidence of glacio-isostatic rebound. *Reviews of Geophysics*, **10**, 849–884, https://doi.org/10.1029/RG010i004p00849

Wan, J.X.W., Gomez, N., Latychev, K. and Han, H.K. 2022. Resolving glacial isostatic adjustment (GIA) in response to modern and future ice loss at marine grounding lines in West Antarctica. *The Cryosphere*, **16**, 2203–2223, https://doi.org/10.5194/tc-16-2203-2022

Wang, K. and Fialko, Y. 2018. Observations and modeling of coseismic and postseismic deformation due to the 2015 M_w 7.8 Gorkha (Nepal) earthquake. *Journal of Geophysical Research: Solid Earth*, **123**, 761–779, https://doi.org/10.1002/2017JB014620

Watson, C., Burgette, R. *et al*. 2010. Twentieth century constraints on sea level change and earthquake deformation at Macquarie Island. *Geophysical Journal International*, **182**, 781–796, https://doi.org/10.1111/j.1365-246X.2010.04640.x

Weertman, J. 1974. Stability of the junction of an ice sheet and an ice shelf. *Journal of Glaciology*, **13**, 3–11, https://doi.org/10.3189/S0022143000023327

Wegener, A. 1915. *The Origin of Continents and Oceans*. Vieweg, Braunschweig, Germany [in German].

Wessel, P., Luis, J.F., Uieda, L., Scharroo, R., Wobbe, F., Smith, W.H.F. and Tian, D. 2019. The Generic Mapping Tools version 6. *Geochemistry, Geophysics, Geosystems*, **20**, 5556–5564, https://doi.org/10.1029/2019GC008515

Whitehouse, P.L. 2018. Glacial isostatic adjustment modelling: historical perspectives, recent advances, and future directions. *Earth Surface Dynamics*, **6**, 401–429, https://doi.org/10.5194/esurf-6-401-2018

Whitehouse, P.L., Bentley, M.J. and Le Brocq, A.M. 2012*a*. A deglacial model for Antarctica: geological constraints and glaciological modelling as a basis for a new model of Antarctic glacial isostatic adjustment. *Quaternary Science Reviews*, **32**, 1–24, https://doi.org/10.1016/j.quascirev.2011.11.016

Whitehouse, P.L., Bentley, M.J., Milne, G.A., King, M.A. and Thomas, I.D. 2012*b*. A new glacial isostatic adjustment model for Antarctica: calibrated and tested using observations of relative sea-level change and present-day uplift rates. *Geophysical Journal International*, **190**, 1464–1482, https://doi.org/10.1111/j.1365-246X.2012.05557.x

Whitehouse, P.L., Gomez, N., King, M.A. and Wiens, D.A. 2019. Solid Earth change and the evolution of the Antarctic Ice Sheet. *Nature Communications*, **10**, 503, https://doi.org/10.1038/s41467-018-08068-y

Wieczerkowski, K., Mitrovica, J.X. and Wolf, D. 1999. A revised relaxation-time spectrum for Fennoscandia. *Geophysical Journal International*, **139**, 69–86, https://doi.org/10.1046/j.1365-246X.1999.00924.x

Wiens, D.A., Shen, W. and Lloyd, A.J. 2021. The seismic structure of the Antarctic upper mantle. *Geological Society, London, Memoirs*, **56**, https://doi.org/10.1144/M56-2020-18

Wilson, T.J., Anandakrishnan, S. *et al*. 2020. Antarctic Network–Polar Earth Observing Network: Achievements from ten years of autonomous measurements. Abstract #C032-002 presented at the 2020 AGU Fall Meeting, 1–17 December 2020, virtual meeting.

Winkelmann, R., Martin, M.A., Haseloff, M., Albrecht, T., Bueler, E., Khroulev, C. and Levermann, A. 2011. The Potsdam Parallel Ice Sheet Model (PISM-PIK) – Part 1: Model description. *The Cryosphere*, **5**, 715–726, https://doi.org/10.5194/tc-5-715-2011

Wobbe, F., Gohl, K., Chambord, A. and Sutherland, R. 2012. Structure and breakup history of the rifted margin of West Antarctica in relation to Cretaceous separation from Zealandia and Bellingshausen plate motion. *Geochemistry, Geophysics, Geosystems*, **13**, Q04W12, https://doi.org/10.1029/2011GC0 03742

Wolstencroft, M., King, M.A. *et al*. 2015. Uplift rates from a new high-density GPS network in Palmer Land indicate significant late Holocene ice loss in the southwestern Weddell Sea. *Geophysical Journal International*, **203**, 737–754, https://doi.org/10.1093/gji/ggv327

Wright, T.J. 2016. The earthquake deformation cycle. *Astronomy & Geophysics*, **57**, 4.20–24.26, https://doi.org/10.1093/astrogeo/atw148

Wu, P. 1992. Deformation of an incompressible viscoelastic flat earth with powerlaw creep: a finite element approach. *Geophysical Journal International*, **108**, 35–51, https://doi.org/10.1111/j.1365-246X.1992.tb00837.x

Wu, P. 2004. Using commercial finite element packages for the study of earth deformations, sea levels and the state of stress. *Geophysical Journal International*, **158**, 401–408, https://doi.org/10.1111/j.1365-246X.2004.02338.x

Wu, P. 2006. Sensitivity of relative sea levels and crustal velocities in Laurentide to radial and lateral viscosity variations in the mantle. *Geophysical Journal International*, **165**, 401–413, https://doi.org/10.1111/j.1365-246X.2006.02960.x

Wu, P. and Peltier, W.R. 1982. Viscous gravitational relaxation. *Geophysical Journal International*, **70**, 435–485, https://doi.org/10.1111/j.1365-246X.1982.tb04976.x

Wu, P. and Peltier, W.R. 1983. Glacial isostatic adjustment and the free air gravity anomaly as a constraint on deep mantle viscosity. *Geophysical Journal International*, **74**, 377–449, https://doi.org/10.1111/j.1365-246X.1983.tb01884.x

Ye, L., Lay, T. *et al*. 2014. Complementary slip distributions of the August 4, 2003 M_w 7.6 and November 17, 2013 M_w 7.8 South Scotia Ridge earthquakes. *Earth and Planetary Science Letters*, **401**, 215–226, https://doi.org/10.1016/j.epsl.2014.06.007

Yuen, D.A. and Peltier, W.R. 1982. Normal modes of the viscoelastic earth. *Geophysical Journal International*, **69**, 495–526, https://doi.org/10.1111/j.1365-246X.1982.tb04962.x

Zhao, C., King, M.A., Watson, C.S., Barletta, V.R., Bordoni, A., Dell, M. and Whitehouse, P.L. 2017. Rapid ice unloading in the Fleming Glacier region, southern Antarctic Peninsula, and its effect on bedrock uplift rates. *Earth and Planetary Science Letters*, **473**, 164–176, https://doi.org/10.1016/j.epsl.2017.06.002

Zhong, S., Paulson, A. and Wahr, J. 2003. Three-dimensional finite-element modelling of Earth's viscoelastic deformation: effects of lateral variations in lithospheric thickness. *Geophysical Journal International*, **155**, 679–695, https://doi.org/10.1046/j.1365-246X.2003.02084.x

Zurbuchen, J. and Simms, A.R. 2019. Late Holocene ice-mass changes recorded in a relative sea-level record from Joinville Island, Antarctica. *Geology*, **47**, 1064–1068, https://doi.org/10.1130/g46649.1